Cell Reports
Medicine

Article

Biguanides antithetically regulate tumor properties by the dose-dependent mitochondrial reprogramming-driven c-Src pathway

Graphical abstract

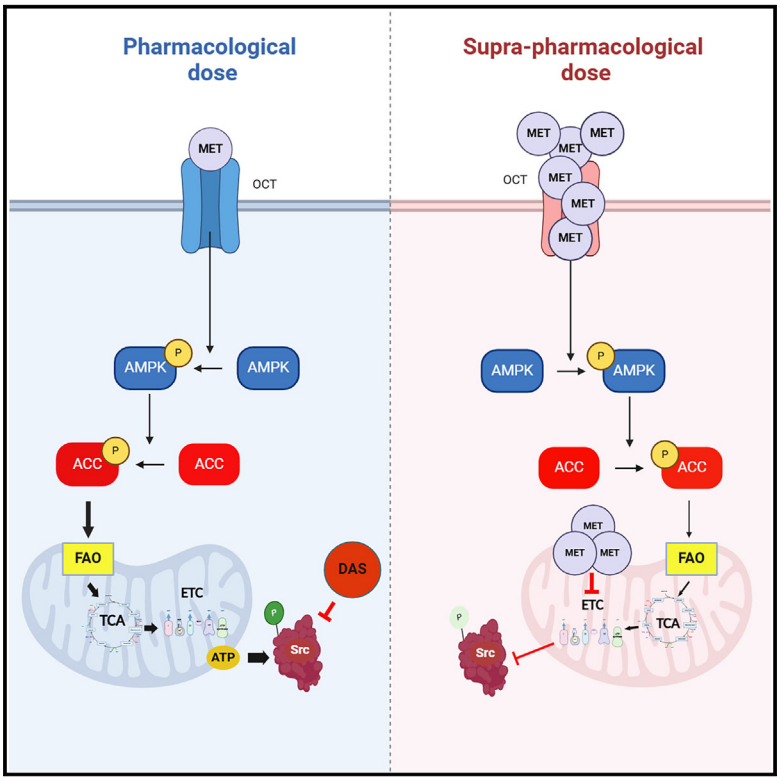

Authors

Jun Hyoung Park, Kwang Hwa Jung, Dongya Jia, ..., José N. Onuchic, Andrei Goga, Benny Abraham Kaipparettu

Correspondence

kaippare@bcm.edu

In brief

Park et al. reveal a mechanism of dose-dependent antithetical regulation of tumor properties by metformin via fatty acid β-oxidation-driven Src pathway and propose a synergistic combination of metformin and dasatinib, which, by repurposing two FDA-approved drugs, could provide the opportunity for rapid clinical translation to treat patients with metastatic TNBC.

Highlights

- Biguanides activate or suppress TNBC progression in a dose-dependent manner
- Biguanides regulate c-Src by the dose-dependent antithetical regulation of AMPK-FAO
- Combination of dasatinib with metformin suppresses TNBC progression and metastasis

Park et al., 2025, Cell Reports Medicine 6, 101941
February 18, 2025
https://doi.org/10.1016/j.xcrm.2025.101941

CellPress

Cell Reports Medicine

CellPress
OPEN ACCESS

Article

Biguanides antithetically regulate tumor properties by the dose-dependent mitochondrial reprogramming-driven c-Src pathway

Jun Hyoung Park,[1] Kwang Hwa Jung,[1] Dongya Jia,[2] Sukjin Yang,[1] Kuldeep S. Attri,[1] Songyeon Ahn,[1] Divya Murthy,[1] Tagari Samanta,[1] Debasmita Dutta,[1] Meron Ghidey,[1] Somik Chatterjee,[1] Seung Yeop Han,[1] Diego A. Pedroza,[3] Abha Tiwari,[1] Joyce V. Lee,[4] Caitlin Davis,[4] Shuting Li,[4] Vasanta Putluri,[3,6] Chad J. Creighton,[5,6] Nagireddy Putluri,[3,6] Lacey E. Dobrolecki,[3] Michael T. Lewis,[3,6] Jeffrey M. Rosen,[3,6] José N. Onuchic,[2] Andrei Goga,[4] and Benny Abraham Kaipparettu[1,6,7,*]

[1]Department of Molecular and Human Genetics, Baylor College of Medicine, Houston, TX 77030, USA
[2]Center for Theoretical Biological Physics, Rice University, Houston, TX 77005, USA
[3]Department of Molecular and Cellular Biology, Baylor College of Medicine, Houston, TX 77030, USA
[4]Department of Cell and Tissue Biology, University of California San Francisco, San Francisco, CA 94143, USA
[5]Department of Medicine, Baylor College of Medicine, Houston, TX 77030, USA
[6]Dan L. Duncan Comprehensive Cancer Center, Baylor College of Medicine, Houston, TX 77030, USA
[7]Lead contact
*Correspondence: kaippare@bcm.edu
https://doi.org/10.1016/j.xcrm.2025.101941

SUMMARY

The biguanide metformin attenuates mitochondrial oxidation and is proposed as an anti-cancer therapy. However, recent clinical studies suggest increased proliferation and fatty acid β-oxidation (FAO) in a subgroup of patients with breast cancer (BC) after metformin therapy. Considering that FAO can activate Src kinase in aggressive triple-negative BC (TNBC), we postulate that low-dose biguanide-driven AMPK-ACC-FAO signaling may activate the Src pathway in TNBC. The low bioavailability of metformin in TNBC xenografts mimics metformin's *in vitro* low-dose effect. Pharmacological or genetic inhibition of FAO significantly enhances the anti-tumor properties of biguanides. Lower doses of biguanides induce and higher doses suppress Src signaling. Dasatinib and metformin synergistically inhibit TNBC patient-derived xenograft growth, but not in high-fat diet-fed mice. This combination also suppresses TNBC metastatic progression. A combination of biguanides with Src inhibitors provides synergy to target metastatic TNBC suffering with limited treatment options.

INTRODUCTION

Triple-negative breast cancer (TNBC) is an aggressive subtype of breast cancer (BC) associated with high metastasis and mortality.[1] Since targeted therapies are limited for patients with TNBC, there is an urgent need to identify promising targets and treatment regimens for TNBC.

Metabolic reprogramming of tumors is increasingly recognized in primary and metastatic sites due to different energy needs and nutrient microenvironments.[2] Aggressive tumors exhibit plasticity in carbon source utilization to support bioenergetic demands.[3] Despite elevated glycolysis in cancer cells, they also utilize mitochondrial respiration to generate significant ATP.[4,5] Our previous studies suggest that reprogramming to mitochondrial fatty acid β-oxidation (FAO) is a dominant metabolic pathway in TNBC.[6,7] Recent studies have identified the presence of a metabolic hybrid state in cancer cells that can utilize both glycolysis and oxidative phosphorylation (OXPHOS) pathways.[8–13] This metabolic hybrid state in cancer cells is critical for tumor progression and adaptation to metastatic niches.[14] Therefore, targeting mitochondrial metabolism remains an attractive treatment option in TNBC therapy.[15]

Biguanides like metformin, the first-line drug of choice for type 2 diabetes mellitus (T2DM), have been recently indicated for anti-cancer therapies. The decreased cancer incidence in diabetic patients on metformin therapy encouraged multiple clinical trials of metformin in various cancers, including TNBC.[16–20] However, metformin failed to reach an effective concentration in tumors and did not inhibit proliferation or provide a survival benefit at clinical doses.[18,21] Thus, it is imperative to find suitable therapeutic combinations to counter the limited effect of biguanides due to poor bioavailability. Suppression of OXPHOS by inhibiting complex I activity of the mitochondrial electron transport chain (ETC) is the primary proposed mechanism for the anti-cancer activity of biguanides.[22,23] Several recent publications discussed the metabolic modulations after biguanide treatments in cancer.[24–26] Importantly, a clinical study by Lord et al. identified two distinct metabolic subgroups of tumors with contrasting

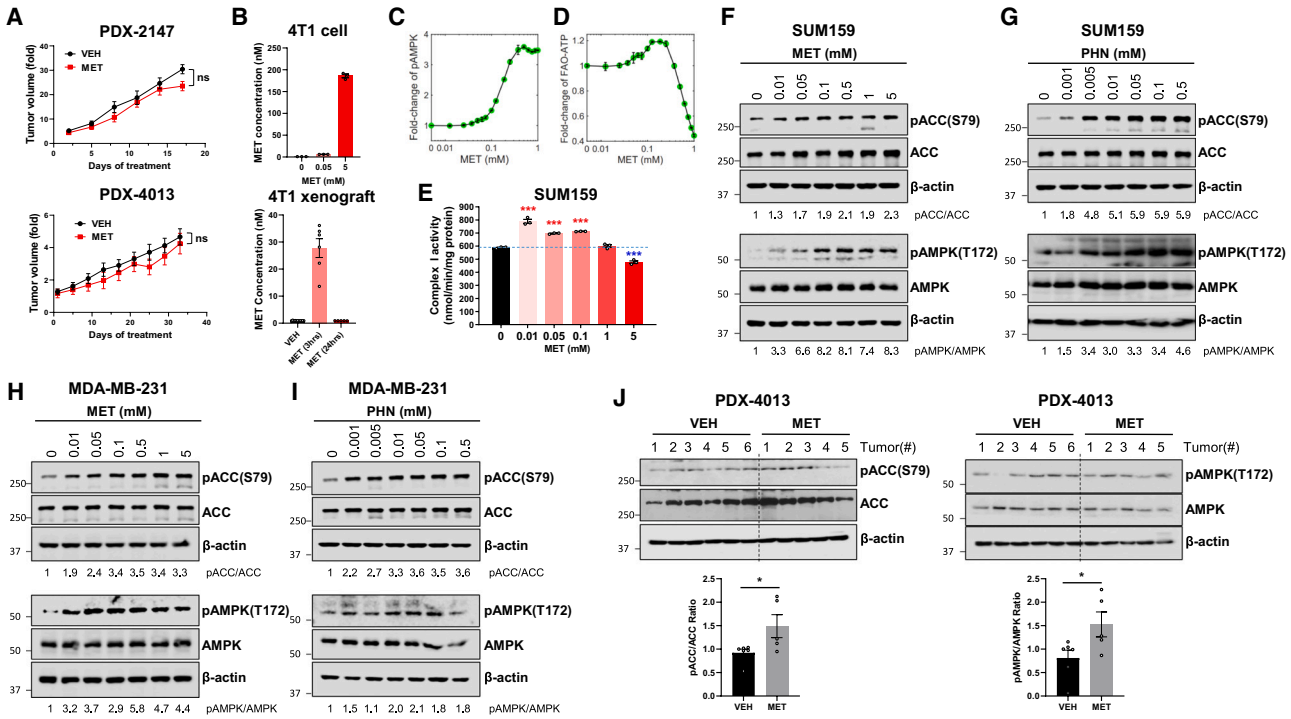

Figure 1. Low-dose biguanides activate the AMPK-ACC pathway in TNBC

(A) Growth curve of PDX-2147 and PDX-4013 tumors in SCID/Beige mice treated with vehicle (VEH) (n = 5) or 200 mg/kg metformin (MET) (n = 5).

(B) Upper: *in vitro* cellular concentration of MET in 4T1 cells after *in vitro* treatment with VEH (n = 3) or MET (n = 3) for 1 day. Lower: *in vivo* tissue concentration of MET in 4T1-xenografts treated with VEH (n = 11) or MET (200 mg/kg) for 7 days in BALB/c mice. Tumors were collected 3 (n = 6) and 24 h (n = 5) after the last MET treatment.

(C and D) Mathematical modeling of the expected fold changes in pAMPK level (C) and ATP production rate from FAO (FAO-ATP) (D) in cancer cells upon treatment with increasing concentration of MET (0.005, 0.0125, 0.025, 0.0375, 0.05, 0.0625, 0.075, 0.1, 0.125, 0.1875, 0.25, 0.375, 0.5, 0.625, 0.75, 0.875, and 1 mM).

(E) Change in ETC complex I activity in SUM159 cells after treatment with increasing concentrations of MET (n = 3). The p value is calculated against 0 mM.

(F–I) Western blot (WB) of pACC (S79) and pAMPK (T172) levels in SUM159 or MDA-MB-231 cells after treatment (1 day) with increasing doses of MET or phenformin (PHN). The ratio of pACC/ACC and pAMPK/AMP is shown below.

(J) WB for pACC (S79) and pAMPK (T172) levels in PDX-4013 tumors treated long term with VEH or MET (200 mg/kg). The below graphs represent the quantification of pACC/ACC and pAMPK/AMPK ratios calculated using ImageJ.

Data on all panels are mean ± SEM. *p < 0.05, **p < 0.01, ***p < 0.001 by two-way ANOVA (A), one-way ANOVA (E), or two-tailed unpaired t test (J).

See also Figure S1.

clinical outcomes in patients with BC on metformin therapy[27]: an OXPHOS transcriptional response (OTR) group with increased transcription of OXPHOS genes and a fluoro-deoxy-D-glucose (FDG) response group with increased 18-FDG uptake. The OTR group of tumors showed increased cell proliferation and drug resistance after metformin therapy.[27] Their further analysis confirmed that metformin treatment of primary BC at therapeutic dosing increased FAO in the OTR tumors, and FAO activation correlated with increased proliferation.[28] Therefore, we hypothesize that identifying companion targets of metabolic reprogramming in TNBC upon biguanide treatment is critical to developing an effective therapeutic combination.

This study presents a comprehensive analysis using multiple models to unravel metformin-induced crosstalk of mitochondria and oncopathway in TNBC. Our data reveal that low-dose metformin reprograms TNBC metabolism to activate the FAO-Src kinase signaling pathway *in vivo*. We propose a therapeutic strategy wherein the clinical dose of metformin synergizes with the Src inhibitor, dasatinib, to effectively regulate tumor growth and metastasis in patients with TNBC.

RESULTS

Biguanides fuel the dichotomous growth of TNBC by modulating the AMPK-FAO pathway

In vivo experiments using TNBC patient-derived xenograft (PDX) and cell line xenograft models suggested that the clinically relevant metformin dose[18] is insufficient in effectively reducing the TNBC tumor growth (Figures 1A, S1A, and S1B). Since biguanides have anti-proliferative effects *in vitro*,[29] we measured metformin concentration in *in vitro* cell line and *in vivo* xenograft models of the 4T1 cell line to compare metformin's *in vitro* and *in vivo* bioavailability. In contrast to *in vitro* treatment, metformin bioavailability of *in vivo* xenografts was rapidly cleared after *in vivo* treatment and reduced to low-dose metformin concentration levels (Figure 1B). Computational modeling of the dose

dependency of metformin using our previously published metabolic model[11] predicted a steady increase of phosphorylation of AMP-activated protein kinase (AMPK), the upstream signaling pathway of FAO, upon increasing metformin concentrations (Figure 1C). However, modeling of FAO-mediated change in ATP levels showed that while lower concentrations were predicted to induce mitochondrial ATP production, higher metformin concentrations suppressed this activity, suggesting a dose-dependent dichotomous metabolic regulation (Figure 1D). We then analyzed the mitochondrial ETC complex I activity in SUM159 cells to validate this dichotomous metabolic regulation. While higher doses of metformin suppressed complex I activity, the lower doses induced complex I activity (Figure 1E). As expected, the tricarboxylic acid cycle enzyme citrate synthase did not follow this activity pattern (Figure S1C). Western blot analyses confirmed that even at very low concentrations, biguanides increase pACC and pAMPK levels in TNBC cells *in vitro* (Figures 1F–1I and S1D–S1G). We then validated the change in phosphorylation of acetyl-CoA carboxylase (ACC) and AMPK in TNBC PDX tissues after long-term metformin therapy. As expected, *in vivo* metformin therapy also induced pAMPK and pACC in TNBC PDX tumors (Figure 1J). AMPK is predominantly regulated by upstream kinases, liver kinase B1 (LKB1), and calcium/calmodulin protein kinase kinase 2 (CaMKK2 or CaMKKβ). LKB1-mediated AMPK activation is a well-studied mechanism in metformin therapy.[30] However, CaMKK2 can also activate AMPK in response to increases in cellular Ca^{2+} without any significant change in ATP/ADP/AMP levels.[31] Thus, we analyzed if CaMKK2 is activated at low doses of biguanides. As expected, we observed an increase of pCaMKK2 in low-dose biguanide-treated cells (Figures S1H and S1I). Since the AMPK-ACC pathway is upstream of FAO,[11,32] we analyzed the FAO pathway after metformin therapy. The mRNA and protein expressions and enzymatic activity of carnitine palmitoyltransferase 1 (CPT1), the rate-limiting enzyme of FAO, were induced at lower doses of biguanides (Figures 2A, S2A, S2B, 2B, and S2C). Since cellular levels of carnitines and its metabolites are an indication of fatty acid shuttle across the mitochondrial membrane and the abundance of FAO intermediates, we performed metabolomic analyses of different carnitine metabolites in SUM159 cells after treating with varying doses of metformin. Metabolomic data suggest that while lower doses of metformin induce, high doses decrease carnitine levels, confirming a dichotomous regulation of FAO activity (Figure 2C). We further validated the metformin-mediated activation of the FAO pathway in previously published RNA sequencing data (GSE95298) generated from metformin-resistant cells.[33] The gene enrichment analysis identified a positive correlation between FAO and the post-metformin-resistant cells (Figure 2D), confirming the activation of the FAO pathway after metformin therapy.

We then analyzed the functional significance of the activation of FAO after treatment with lower doses of biguanides in TNBC cells. Interestingly, while higher doses of biguanide have an anti-proliferative effect as expected, lower doses of biguanides promoted TNBC cell growth (Figures 2E–2H and S2D). To confirm the necessity of functional mitochondrial ETC in this dichotomous cellular growth after biguanide therapy, we compared the clonogenic potential between the wild-type SUM159 cells and its mitochondrial (mt) DNA-depleted Rho0 cells.[6] Lack of increase in colony formation after low-dose metformin therapy in the Rho0 cells confirmed that low concentration-induced clonogenic potential requires functional mitochondria (Figures 2I and S2E). We then performed a similar analysis in *trans*-mitochondrial cybrid models,[6] where benign (C-A1N4) and cancer (C-SUM159) mitochondria were transferred to the SUM159 Rho0 cells. As expected, compared to C-A1N4, the low-dose metformin-induced clonogenic potential was more evident in C-SUM159 with cancer mitochondria (Figure 2J). We also validated the clonogenic potential in MTB-TOM basal BC cells that contain doxycycline (DOX)-inducible Myc that activates mitochondrial FAO activity (Figures S2F and S2G).[7] Lower doses of metformin significantly enhanced colony formation in the presence of DOX, suggesting a critical role for FAO in low-dose metformin-induced colony formation in TNBC (Figure 2K). Collectively, our data suggest that lower doses of biguanides activate the AMPK-ACC-FAO pathway and induce TNBC growth.

Inhibition of FAO enhances the anti-cancer effects of biguanides in TNBC

Since lower doses of biguanides induce FAO and tumor properties in TNBC, we investigated if the FAO inhibitor etomoxir (ETX) would enhance the anti-cancer function of biguanides. Utilizing multiple approaches such as clonogenic (proliferation), mammosphere (stemness), and wound healing (metastasis) assays in human and mouse TNBC cells (SUM159, MDA-MB-231, SUM149, and 4T1), we confirmed a significant reduction in TNBC tumor properties when ETX was treated in combination with biguanides (Figures 3A–3F and S3A–S3G). To rule out the potential off-target effects of ETX, we validated this finding using a clinically approved FAO inhibitor, ranolazine (RNL). As observed with ETX, the combination of metformin and RNL also considerably reduced the clonogenic potential of SUM159 and MDA-MB-231(Figures S4A and S4B). To avoid any FAO-targeting drugs, we used a genetic approach by short hairpin RNA (shRNA)-mediated knockdown (KD) of CPT1 and CPT2 genes in MDA-MB-231 cells to deplete CPT1 or CPT2, the essential transporters of long-chain fatty acids, into the mitochondria (Figure 4A). As observed with the FAO inhibitors, compared to the scrambled shRNA cells, KD of CPT1 or CPT2 gene significantly enhanced the anti-cancer effect of biguanides (Figures 4B, 4C, and S4C–S4E). The combination of metformin with ETX also significantly reduced the organoid number in two PDX-derived organoids (PDXOs) generated from BCM-3936 and BCM-3561 TNBC PDX models (PDXO-3936 and PDXO-3561) (Figures 4D and 4E). The combination effect of metformin and ETX on *in vivo* tumor growth was confirmed using the BCM-4013 TNBC PDX model (Figure 4F). Overall, our data indicate that preventing FAO activation is critical for biguanide's anti-cancer activity in TNBC.

Biguanide-induced FAO activates the Src kinase pathway

Our previous studies demonstrated that metabolic reprogramming to FAO in TNBC activates Src kinase by Y419 autophosphorylation (pSrc(Y419)).[6] Analysis of BC data from The Cancer Genome Atlas (TCGA) showed a strong positive correlation

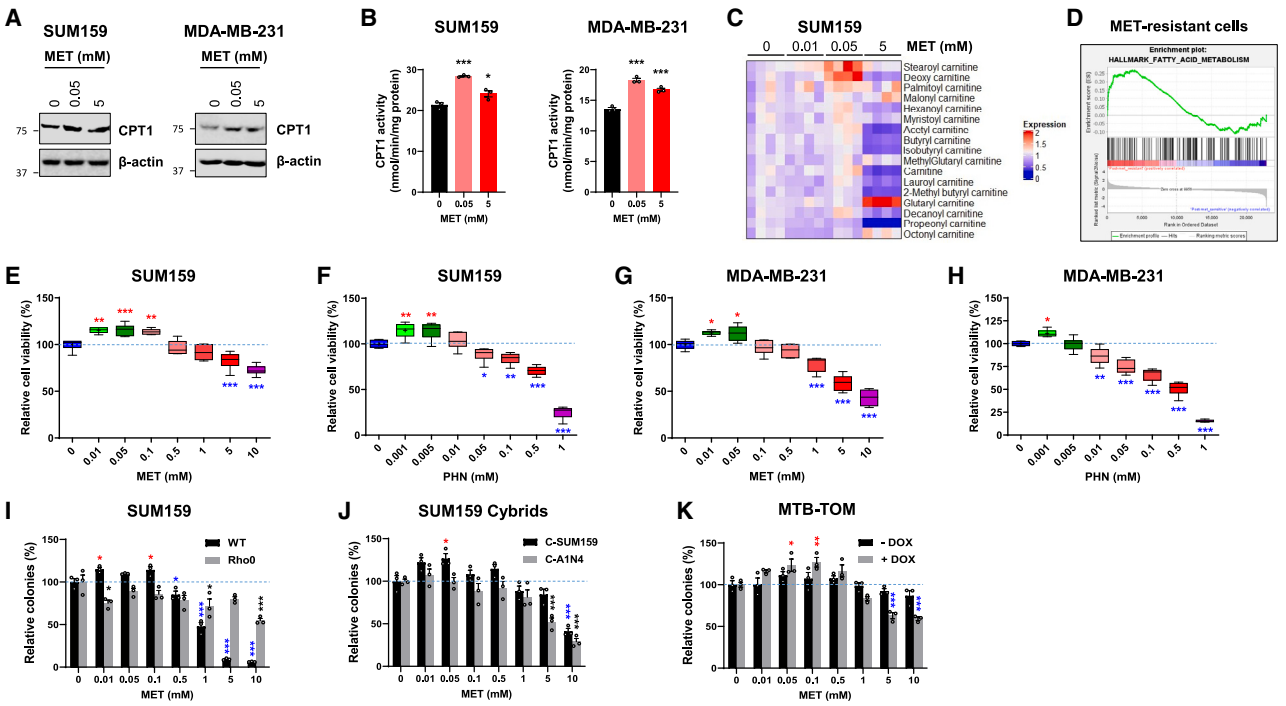

Figure 2. Low-dose biguanides activate mitochondrial FAO and cell growth in TNBC

(A) WB of CPT1 in SUM159 and MDA-MB-231 cells treated with VEH or MET for 1 day.

(B) CPT1 enzymatic activity assay after treatment with VEH or MET for 1 day (n = 3). The p value is calculated against 0 mM.

(C) Metabolomic analysis of carnitine metabolites in SUM159 cells treated with low and high doses of MET (n = 4).

(D) Gene set enrichment analysis of the post-MET-resistant cells (GSE95298) showing an enrichment of FAO pathway in MET-resistant cells.

(E–H) SRB cell viability assay of SUM159 or MDA-MB-231 cells treated with VEH or increasing concentrations of MET or PHN (n = 6). p value is calculated against 0 mM.

(I) Quantification of the relative percentages of colonies from the clonogenic assay of SUM159 parental cells and mtDNA-depleted SUM159 Rho0 cells after treatment with increasing concentrations of MET (n = 3). p value is calculated against 0 mM.

(J) Quantification of the relative percentages of colonies from the clonogenic assay of SUM159 *trans*-mitochondrial cybrid (C-) models. C-A1N4 has benign (A1N4) and C-SUM159 has cancer (SUM159) mitochondria. Cybrids were treated with increasing concentrations of MET (n = 3). p value is calculated against 0 mM.

(K) Quantification of the relative percentages of colonies from the clonogenic assay of DOX-inducible MYC-driven MTB-TOM TNBC cells. Cells were treated with increasing concentrations of MET (n = 3) in the presence or absence of DOX. p value is calculated against 0 mM.

Data on all panels are mean ± SEM. $^{*}p < 0.05$, $^{**}p < 0.01$, $^{***}p < 0.001$ by one-way ANOVA (B and E–K).

See also Figure S2.

between AMPK and Src signatures (Figure 5A). Since higher doses of metformin directly inhibit ETC complex I,[34] we performed an RNA sequencing analysis after treatment with a high concentration (5 mM) of metformin in MDA-MB-231 cells. Transcriptomic data confirmed that Src signature is one of the most significantly downregulated pathways after high-dose metformin treatment in TNBC cells (Figure 5B). Higher dose of metformin also affected other pathways including the cell cycle, Wnt, YAP1, and Notch pathway (Figures 5B and S5A). Since we previously confirmed the significance of c-Src as a major downstream oncopathway in TNBC,[6] we validated the activation of pSrc(Y419) after treatment with different metabolic inhibitors. While the glycolytic inhibitor 3-bromopyruvate (3BP) shows limited downregulation, biguanides (metformin and phenformin), ETC inhibitors (rotenone and antimycin A), and the FAO inhibitor (ETX) considerably reduced pSrc(Y419) levels (Figure 5C). A combination of biguanide and ETX further reduced pSrc(Y419) levels in TNBC cells (Figures S5B and S5C).

We then analyzed if lower doses of biguanide-induced FAO also activate c-Src. In line with the activation of the AMPK-ACC-FAO pathway shown in Figures 1 and 2, lower doses of biguanides increased and higher doses decreased pSrc(Y419) in TNBC cells (Figures 5D, 5E, and S5D). To confirm the specificity of biguanides in regulating Src phosphorylation, we tested the effect of two drugs recently approved for treating T2DM. Treatment with tirzepatide, which is a glucagon-like peptide-1 (GLP-1) and glucose-dependent insulinotropic polypeptide receptor agonist,[35] or canagliflozin, a sodium-glucose co-transporter 2 (SGLT2) inhibitor,[36] did not inhibit pSrc(Y419) in TNBC cells (Figure S5E). Moreover, tirzepatide or canagliflozin did not affect the low-dose metformin-induced pSrc(Y419) in TNBC cells (Figure S5F). We then evaluated the PDX tumors harvested after a long-term *in vivo* treatment with vehicle or metformin. Tumor analyses of pSrc(Y419) suggest that metformin-treated *in vivo* PDX tumors mimicked the low-dose biguanide-treated *in vitro* cell models with increased pSrc(Y419) levels compared

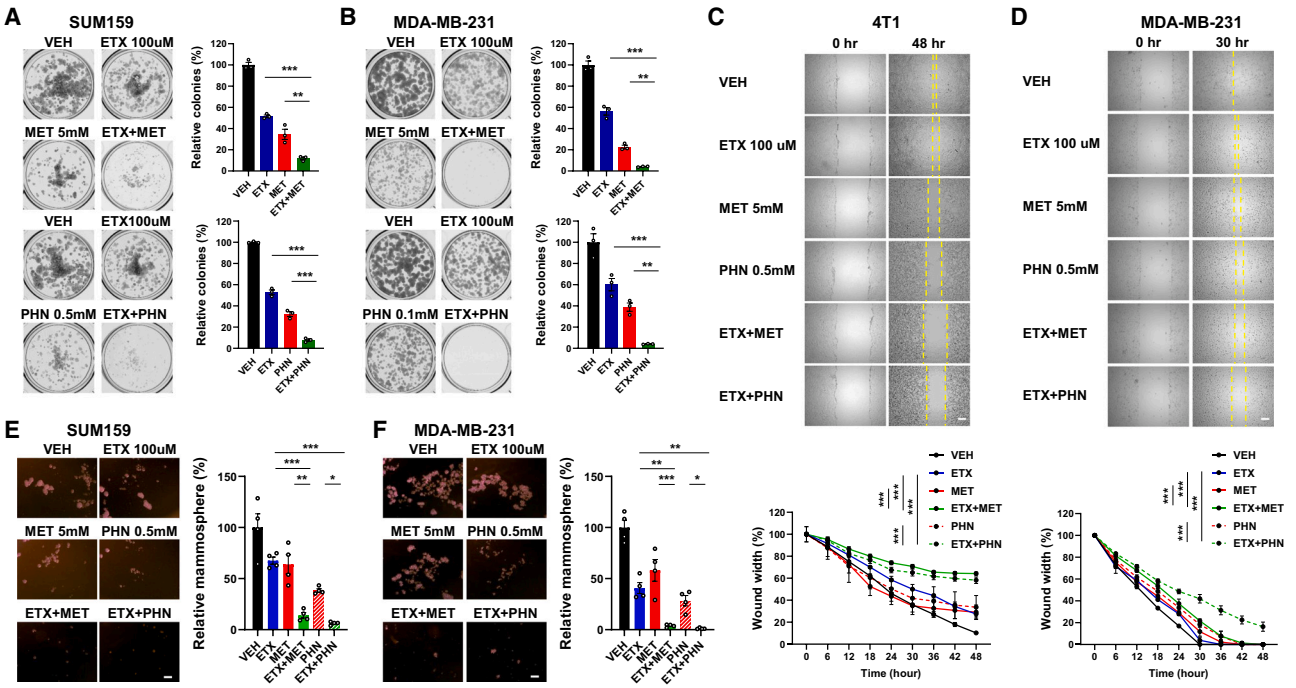

Figure 3. Inhibition of FAO potentiates the anti-cancer effect of biguanides

(A and B) Representative images and the quantification of clonogenic assay of SUM159 (A) and MDA-MB-231 (B) cells treated with etomoxir (ETX) and biguanides ($n = 3$).

(C and D) Representative images and the quantification of time-lapse images of wound healing assays using the Cytation 5 cell imager. 4T1 (C) and MDA-MB-231 (D) cells treated with ETX and biguanides ($n = 3$). Scale bar indicates 200 μm.

(E and F) Representative images and quantification of mammosphere assay of SUM159 (E) and MDA-MB-231 (F) cells treated with ETX and MET ($n = 4$). Scale bar indicates 400 μm.

Data on all panels are mean ± SEM. *$p < 0.05$, **$p < 0.01$, ***$p < 0.001$ by one-way ANOVA (A, B, E, and F) or two-way ANOVA (C and D).

See also Figure S3.

to the vehicle-treated tumors (Figure 5F). These data support metformin's limited *in vivo* tumor bioavailability, as shown in Figure 1B.

A combination of metformin and dasatinib synergistically inhibits *in vivo* tumor growth and metastasis of TNBC

We analyzed if a combination of metformin with an Src inhibitor is a beneficial therapeutic option in TNBC. Combining biguanides with the clinically approved Src inhibitor (Figure S5G), dasatinib, significantly inhibited the clonogenic potential (colony formation assay), metastasis (wound healing assay), migration (transwell assay), tumorigenicity (soft agar colony formation), and stemness (mammosphere assay) properties in multiple TNBC cell lines (Figures 6A–6H and S6A–S6G). We also confirmed that the combination of biguanides and dasatinib induces a cellular apoptotic marker (cleaved PARP) and inhibits the cell proliferation marker CDK4 (Figure S6H).

Considering the excellent *in vitro* combination effect of biguanides and the Src inhibitor in cell lines, we validated this combination *ex vivo* in organoids using multiple TNBC PDXO models generated from TNBC PDX models. As expected, the combination of metformin with dasatinib significantly decreased the PDXO numbers compared to single-drug therapy (Figures 7A, 7B, and S7A–S7C). We then confirmed this finding *in vivo* using TNBC PDX models. As expected, treatment with a combination of metformin and dasatinib significantly decreased tumor growth and significantly prolonged the survival (to the endpoint) of TNBC PDX-bearing mice (Figures 7C, 7D, 7F, and 7G). However, no considerable body weight change was observed (Figures S7D and S7E). Synergism analysis confirmed that the combination of metformin and dasatinib is a synergistic combination in TNBC (Figures 7E and 7H). Immunohistochemistry (IHC) analysis confirmed a significantly reduced proliferative index in combination-treated tumors (Figures 7I and S7F). Several reports have shown that a higher dietary fat intake remarkably increases death from BC.[37–40] Since FAO is a key regulator of Src, we hypothesized that the synergistic effect of metformin and dasatinib observed in mice with a regular diet may not be feasible in a high-fat diet scenario due to the increased fat transport. As expected, the high-fat diet attenuated the synergistic effect and the survival benefit of biguanides and Src inhibitor combination therapy in the TNBC PDX model (Figures 7J–7L). We then evaluated the significance of this combination in TNBC metastasis using the 4T1 spontaneous metastasis model. After a short-term drug therapy, the primary tumors were resected at a similar tumor size, and lung metastasis was evaluated after treatment for about 3 weeks (Figures S7G and S7H). Importantly, the

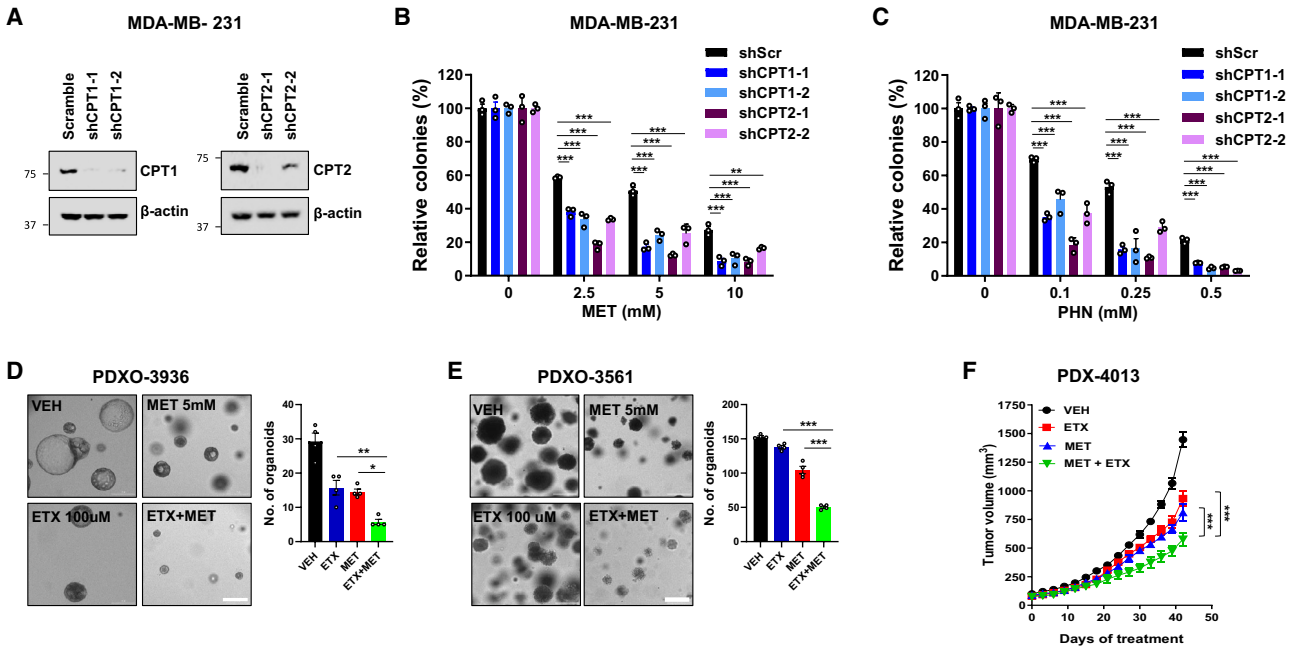

Figure 4. Genetic or *in vivo* suppression of FAO enhances the anti-cancer effect of biguanides

(A) WB confirming the shRNA-mediated stable knockdown of CPT1 and CPT2 proteins in MDA-MB-231 cells.

(B and C) Quantification of the relative percentages of colonies from the clonogenic assay of control (shScr), CPT1, or CPT2 shRNA-transfected MDA-MB-231 cells. Cells were treated with MET (B) or PHN (C) (n = 3).

(D and E) Representative images and quantification (≥200 μm) of PDXO-3936 (D) and PDXO-3561 (E) treated with ETX and MET (n = 4). Scale bar indicates 300 μm.

(F) Tumor growth curve of PDX-4013 in SCID/Beige mice treated with ETX (50 mg/kg) and MET (200 mg/kg) (n = 6).

Data on all panels are mean ± SEM. *p < 0.05, **p < 0.01, ***p < 0.001 by one-way ANOVA (B–E) or two-way ANOVA (F).

See also Figure S4.

combination of metformin and dasatinib dramatically reduced lung metastatic nodules compared to the single drugs (Figures 7M and 7N). Overall, our combinatory approach utilizing the mitochondria-oncopathway crosstalk provides a repurposing significance for two established and economically viable drugs in targeting metastatic TNBC that currently suffers from limited therapeutic options.

DISCUSSION

There was substantial enthusiasm for repurposing metformin to prevent or treat TNBC based on initial reports indicating that patients with T2DM treated with metformin were observed to experience reduced TNBC incidence, increased time to develop cancer, reduced mortality from cancer, or reduced risk of distant metastases.[41] However, a different population-based study reported that a history of diabetes, use of diabetes medications, and use of metformin specifically were positively associated with TNBC incidence.[42] These conflicting findings raise the concern that metformin treatment at certain doses possibly increases the risk of at least some patients with TNBC.

As a single agent, clinically relevant doses of metformin (~35 mg/kg) routinely used to treat patients with T2DM have failed to consistently provide anti-neoplastic activity in mouse models.[43,44] Only supra-pharmacological metformin doses ranging from 150 to 500 mg/kg/day in mice have shown substantial anti-cancer effects *in vivo*.[45,46] Another biguanide, phenformin, showed great promise but failed in clinical trials because of lactic acidosis and increased cardiac mortality.[47] Thus, there is an urgent need to identify the resistance mechanisms behind metformin therapy in TNBC and develop therapies of clinically accepted doses of metformin with scientifically relevant and clinically feasible combination drugs that are relevant in TNBC.

Overall, the findings from this study confirm that the metformin dose-dependent dichotomous regulation of FAO and mitochondrial ETC function is critical in activating the Src pathway and tumor progression in TNBC. Our findings concur with a clinical study conducted in patients with primary BC, in which transcriptomic and metabolomic analyses of paired tissues were collected before and after metformin therapy.[27] Tumor analysis identified two types of tumors post treatment with increased OXPHOS or glycolysis signature.[27] Though that study was not exclusively focused on the TNBC subtype, a follow-up publication[28] confirmed that an increase in the expression of a composite mitochondrial FAO gene expression profile in the OXPHOS group correlated with an increased proliferation gene signature. This study confirms this clinical finding of increased proliferation after low-dose metformin therapy and suggests that the increased FAO from low tumor availability of metformin induces Src oncopathway after *in vivo* metformin therapy.

CellPress
OPEN ACCESS

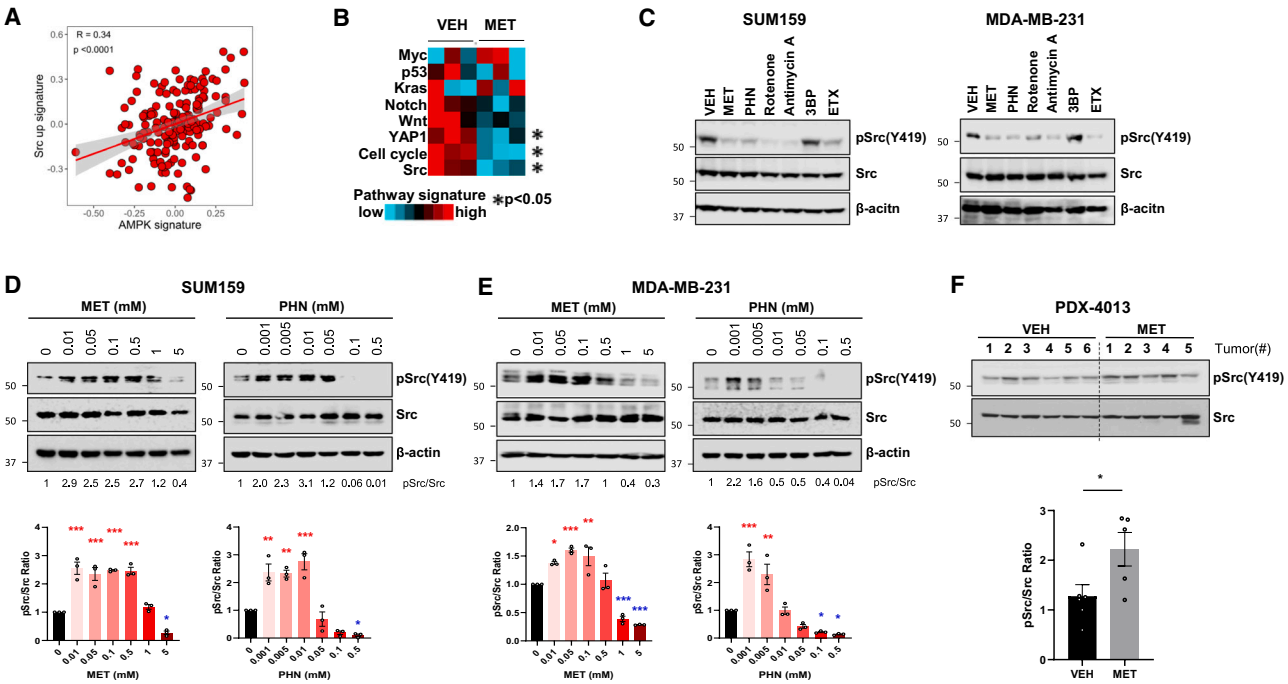

Figure 5. Biguanide-induced FAO activates Src kinase

(A) Analysis of BC patient data from TCGA suggests that Src upregulated gene signatures are positively correlated with AMPK signature.

(B) Oncopathway signature analysis of RNA-seq data (GSE222767) from VEH or MET (5 mM)-treated MDA-MB-231 cells for 1 day (n = 3).

(C) WB of pSrc(Y419) in SUM159 and MDA-MB-231 cells treated for 1 day with metabolic inhibitors. MET (5 mM) and PHN (0.5 mM), ETC complex I inhibitor: rotenone (1 μM), complex III inhibitor: antimycin A (10 μM), glycolysis inhibitor: 3BP (10 μM), and FAO inhibitor: ETX (100 μM).

(D and E) WB of pSrc(Y419) in SUM159 (D) or MDA-MB-231 (E) cells after treatment (1 day) with increasing doses of MET or PHN. The average ratios of pSrc/Src from three independent WB experiments calculated using ImageJ are shown below.

(F) WB of pSrc(Y419) and quantification of pSrc(Y419)/Src ratio of PDX-4013 tumors treated with MET (200 mg/kg). *This experiment was performed together with the WB data shown in Figure 1J.

Data on all panels are mean ± SEM. *p < 0.05, **p < 0.01, ***p < 0.001 by one-way ANOVA (D and E) or two-tailed unpaired t test (B and F).

See also Figure S5.

We have previously reported that FAO activates Src oncopathway in TNBC by autophosphorylation of Src at Y419.[6] The discovery of the low-dose metformin-induced AMPK-ACC-FAO-Src axis in this study has major therapeutic potential for TNBC. The Src pathway is one of the most frequently upregulated pathways in TNBC tumors[48] and is also associated with increased metastasis.[49] Dasatinib is among the most clinically studied Src inhibitors.[50,51] However, its effect as a single drug failed to provide an overall benefit in multiple clinical trials.[52–56]

Metformin is well known to exert its effects by multiple pathways, including inhibition of mitochondrial respiration and AMPK-dependent inhibition of hepatic gluconeogenesis.[18,47] While its exact mechanisms in patients with cancer remain controversial, inhibition of mitochondrial ETC complex I is regarded as the major anti-cancer mechanism.[17] Complex I inhibition alters AMP/ATP and ADP/ATP ratio to activate AMPK signaling.[57] Our dose-escalation experiments suggested that a low dose of metformin is sufficient to activate the AMPK-ACC pathway to induce FAO and ETC functions in TNBC. Thus, the activation of AMPK-ACC-FAO signaling by metformin in TNBC occurs without compromising ETC activity. Studies reported alternate mechanisms of AMPK activation regardless of the mitochondrial AMP levels.[45,58,59] A recent study by Ma et al. reported that metformin binds to the presenilin enhancer 2 (PEN2) subunit of γ-secretase present in the lysosomes at clinical doses leading to the activation of AMPK without any change in AMP levels.[60] Similarly, a major upstream kinase of AMPK, the calcium-triggered signaling kinase CaMKK2, is also known to activate AMPK without sensing the cellular energy status.[31] Interestingly, previous studies have shown that metformin treatment can induce calcium signaling.[61,62] Thus, low-dose metformin may not require the inhibition of ETC complex I to activate AMPK-ACC signaling. *In vitro* treatment with the GLP-1 agonist tirzepatide and the SGLT2 inhibitor canagliflozin did not inhibit Src phosphorylation in TNBC cells. Moreover, they did not influence the low-dose metformin-induced pSrc (Y419) in combination treatment. However, while these T2DM drugs likely do not have the same direct effects as metformin on TNBC cells, further *in vivo* studies may be necessary to confirm if they will overshadow metformin's indirect effects on Src regulation.

Our finding is very important from an *in vivo* therapeutic point because the concentration of metformin available within the tumor cells is a critical deciding factor for its pro- or anti-tumor properties in TNBC. Measuring tumor concentration of metformin suggests that even after 3 h, the concentration of metformin in the xenografts was lower than the observed

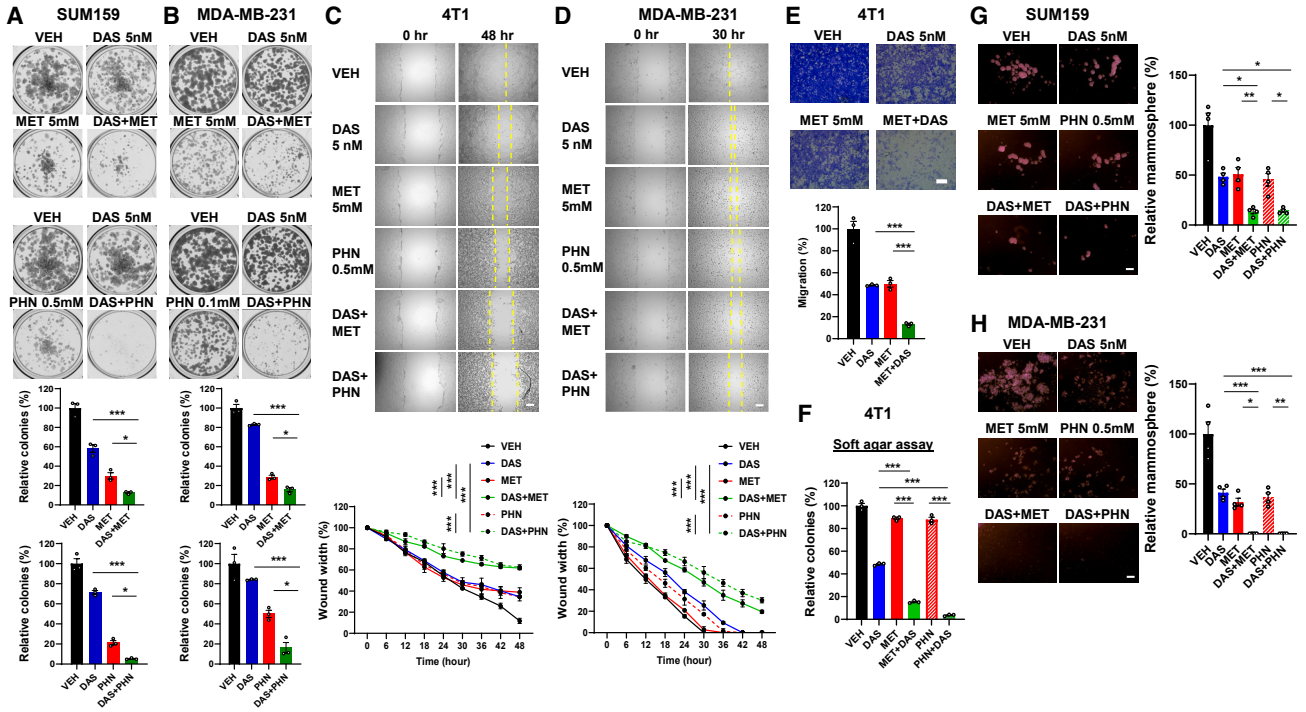

Figure 6. Dasatinib potentiates the anti-cancer effect of biguanides

(A and B) Representative images and the quantification of clonogenic assay of SUM159 (A) and MDA-MB-231 (B) cells treated with dasatinib (DAS) and biguanides ($n = 3$).

(C and D) Representative images and the quantification of time-lapse images of wound healing assays using the Cytation 5 cell imager. 4T1 (C) and MDA-MB-231 (D) cells treated with DAS and biguanides ($n = 3$). Scale bar indicates 200 μm.

(E) Representative images and quantification of transwell migration assay of 4T1 cells treated with DAS and MET ($n = 3$). Scale bar indicates 200 μm.

(F) The quantification of soft agar colony assay of 4T1 cells treated with DAS and biguanides ($n = 3$).

(G and H) Representative images and quantification of mammosphere assay of SUM159 (G) and MDA-MB-231 (H) cells treated with DAS and biguanides ($n = 4$). Scale bar indicates 400 μm.

Data on all panels are mean ± SEM. $^{*}p < 0.05$, $^{**}p < 0.01$, $^{***}p < 0.001$ by one-way ANOVA (A, B, and E–H) or two-way ANOVA (C–D).

See also Figure S6.

metformin-driven activation of the FAO-Src axis *in vitro*. A high dose of dasatinib has side effects, and many clinical trials in solid tumors had to reduce the dose of dasatinib to improve tolerability.[50,51] We used the lowest reported doses (10–20 mg/kg) of dasatinib compared to other preclinical studies (10–50 mg/kg).[63–65] Even low-dose dasatinib provides a synergistic effect when combined with metformin in TNBC. Thus, this study reveals that a synergistic combination of low-dose dasatinib with a clinically relevant dose of metformin, one of the most prescribed and inexpensive drugs with an established safety profile, has high clinical significance in TNBC therapy.

To conclude, considering the limited effective therapeutic options currently available for patients with TNBC, our study provides potentially faster clinical translation by repurposing two Food and Drug Administration-approved drugs that failed to provide clinical benefit when used as monotherapy.

Limitations of the study

AMPK pools have been known to exist in multiple intracellular compartments.[66] This study does not provide the detailed mechanisms of low-dose metformin-mediated AMPK activation without inhibiting the OXPHOS activity. Moreover, the role of low-dose metformin on CaMKK2 activation also requires further investigation. The effect of metformin on other Src family kinases in TNBC has not been investigated in this manuscript. Though preclinical experiments in this manuscript show a lack of inhibition of Src autophosphorylation after *in vivo* metformin therapy, this needs further validation in tissues from patients with TNBC. While the GLP-1 agonist or SGLT2 inhibitor did not inhibit Src phosphorylation *in vitro*, further *in vivo* studies are required to confirm the systemic effect of these drugs on Src regulation. The role of immune factors that contribute to the synergistic effect of metformin and dasatinib has not been addressed in this manuscript. Further studies are necessary to understand the role of metformin and its combination with Src inhibitors in regulating the tumor microenvironment of TNBC.

RESOURCE AVAILABILITY

Lead contact

Further information and requests for resources and reagents should be directed to and will be fulfilled by the lead contact, Benny Abraham Kaipparettu (kaippare@bcm.edu).

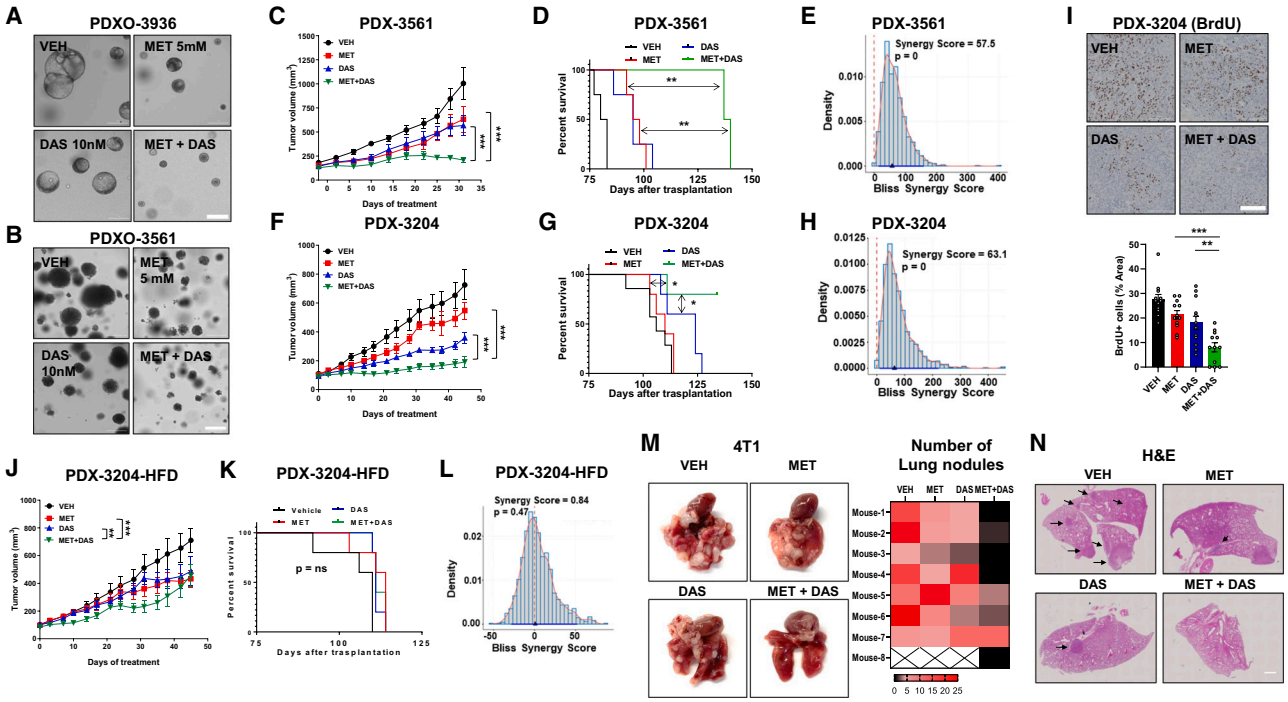

Figure 7. MET and DAS combination synergistically regresses tumor growth and metastasis

(A and B) Representative images of PDXO-3936 ($n = 4$) (A) and PDXO-3561 ($n = 4$) (B) treated with MET and DAS (These experiments were performed together with Figures 4D and 4E, respectively). Scale bar indicates 300 μm.

(C–E) Tumor growth curves (C), tumor endpoint survival graph (D), and the synergism analysis (E) of PDX-3561 in SCID/Beige mice were treated with MET (200 mg/kg) and DAS (10 mg/kg) ($n = 4$).

(F–H) Tumor growth curves (F), tumor endpoint survival graph (G), and the synergism analysis (H) of PDX-3204 in SCID/Beige mice were treated with MET (200 mg/kg) and DAS (20 mg/kg) (n = VEH: 7 and drugs: 5).

(I) Representative IHC images and quantification of BrdU (G) staining of PDX-3204 tumor tissues from Figure 4F ($n = 3$ tumors × 4 representative areas). Scale bar indicates 200 μm.

(J–L) Tumor growth curves (J), tumor endpoint survival graph (K), and the synergism analysis (L) of PDX-3204 in SCID/Beige mice fed with high-fat diet (HFD) were treated with MET (200 mg/kg) and DAS (20 mg/kg) ($n = 5$).

(M) Representative images of spontaneous lung metastasis of 4T1 cells after the BALB/c mice treated with MET (200 mg/kg) and DAS (20 mg/kg). The heatmap represents the number of lung metastatic nodules in the individual mouse. VEH, MET and DAS ($n = 7$), and its combination ($n = 8$).

(N) H&E images of lungs after *in vivo* spontaneous lung metastasis from 4T1 cells. The arrows indicate metastatic nodules. Scale bar indicates 1 mm.

Data on all panels are mean ± SEM. *$p < 0.05$, **$p < 0.01$, ***$p < 0.001$ by one-way ANOVA (I), two-way ANOVA (C, F, and J), bliss method (E, H, and L), or Mantel-Cox test (D, G, and K).

See also Figure S7.

Materials availability

All unique/stable reagents generated in this study are available from the lead contact with a completed materials transfer agreement.

Data and code availability

- RNA-seq data have been deposited at NCBI GEO, and metabolomics data have been deposited at the Metabolomics Workbench (https://doi.org/10.21228/M8CC1G). Accession numbers are listed in the key resources table. Data generated in this study are available from the lead contact upon request.
- This paper does not report the original code.
- Any additional information required to reanalyze the data in this work paper is available from the lead contact upon request.

ACKNOWLEDGMENTS

We thank Ms. Kim and Mishra for her technical support. The study is supported by National Cancer Institute (NCI) (CA253445, CA234479, CA235113 [B.A.K.], CA234479-S1 [M.G.], CA223817 [A.G.], and CA148761 [J.M.R.]), U.S. Department of Defense (DOD) (W81XWH-18-1-0714 [B.A.K. and A.G.], HT94252410012 [B.A.K.], and W81XWH-21-1-0774 [A.G.]), and Marfan Foundation (Endeavor grant to A.G.). D.A.P. is supported by the T32 award. N.P. and Metabolomics Core Facility are supported by Cancer Prevention Research Institute of Texas RP210227, an NCI Cancer Center Support P30 CA125123 grant (to C. Kent Osborne), and Dan L Duncan Comprehensive Cancer Center. M.T.L. and L.E.D. are supported by NCI grants U54 CA224076 and P30 CA125123 and a Core Facility Support Grant from the CPRIT RP220646. J.N.O. is a CPRIT Scholar in Cancer Research sponsored by the Cancer Prevention and Research Institute of Texas and works at the Center for Theoretical Biological Physics supported by the NSF (grants PHY-2019745 and PHY-2210291) and by the Welch Foundation (grant C-1792). Metabolomics Workbench is supported by NIH grants U2C-DK119886 and OT2-OD030544.

AUTHOR CONTRIBUTIONS

B.A.K. and J.H.P. conceived the idea. J.H.P., K.H.J., D.J., S.Y., K.S.A., S.A., T.S., D.D., M.G., S.C., S.Y.H., D.A.P., J.V.L., C.D., S.L., and A.T. performed

the experiments and analyzed the data under the supervision of B.A.K., A.G., J.N.O., and J.M.R. RNA-seq analyses were conducted by C.J.C. Metabolomics was performed by N.P., V.P., and the metabolomic core facility. PDX models were developed by M.T.L., L.E.D., and the PDX core facility. J.H.P., K.S.A., D.M., and B.A.K. wrote the manuscript with the help of other co-authors.

DECLARATION OF INTERESTS

The authors declare no competing interests.

STAR★METHODS

Detailed methods are provided in the online version of this paper and include the following:

- KEY RESOURCES TABLE
- EXPERIMENTAL MODEL AND STUDY PARTICIPANT DETAILS
  - Cells
  - PDX-derived organoid (PDXO)
  - Animal experiments
- METHOD DETAILS
  - Mathematical modeling
  - The correlation of Src and AMPK signature
  - Protein isolation and western blot analysis
  - RNA isolation and qRT-PCR
  - RNA-seq analysis
  - Seahorse analysis
  - Cell viability assay
  - Wound healing assay
  - Proliferation assay
  - Clonogenic assay
  - Soft agar colony formation assay
  - Mammosphere forming assay
  - Migration assay
  - Immunohistochemistry staining
  - CPT1 activity assay
  - Complex I activity assay
  - Mitochondrial (mt) DNA copy number
  - PDXO generation
  - Quantification of metformin
  - Metabolomics
- QUANTIFICATION AND STATISTICAL ANALYSIS

SUPPLEMENTAL INFORMATION

Supplemental information can be found online at https://doi.org/10.1016/j.xcrm.2025.101941.

Received: May 10, 2024
Revised: September 27, 2024
Accepted: January 13, 2025
Published: February 10, 2025

REFERENCES

1. Yin, L., Duan, J.J., Bian, X.W., and Yu, S.C. (2020). Triple-negative breast cancer molecular subtyping and treatment progress. Breast Cancer Res. *22*, 61. https://doi.org/10.1186/s13058-020-01296-5.
2. Roshanzamir, F., Robinson, J.L., Cook, D., Karimi-Jafari, M.H., and Nielsen, J. (2022). Metastatic triple negative breast cancer adapts its metabolism to destination tissues while retaining key metabolic signatures. Proc. Natl. Acad. Sci. USA *119*, e2205456119. https://doi.org/10.1073/pnas.2205456119.
3. Ashton, T.M., McKenna, W.G., Kunz-Schughart, L.A., and Higgins, G.S. (2018). Oxidative Phosphorylation as an Emerging Target in Cancer Therapy. Clin. Cancer Res. *24*, 2482–2490. https://doi.org/10.1158/1078-0432.CCR-17-3070.
4. LeBleu, V.S., O'Connell, J.T., Gonzalez Herrera, K.N., Wikman, H., Pantel, K., Haigis, M.C., de Carvalho, F.M., Damascena, A., Domingos Chinen, L.T., Rocha, R.M., et al. (2014). PGC-1alpha mediates mitochondrial biogenesis and oxidative phosphorylation in cancer cells to promote metastasis. Nat. Cell Biol. *16*, 992–1003. https://doi.org/10.1038/ncb3039.
5. Tan, A.S., Baty, J.W., Dong, L.F., Bezawork-Geleta, A., Endaya, B., Goodwin, J., Bajzikova, M., Kovarova, J., Peterka, M., Yan, B., et al. (2015). Mitochondrial genome acquisition restores respiratory function and tumorigenic potential of cancer cells without mitochondrial DNA. Cell Metab. *21*, 81–94. https://doi.org/10.1016/j.cmet.2014.12.003.
6. Park, J.H., Vithayathil, S., Kumar, S., Sung, P.L., Dobrolecki, L.E., Putluri, V., Bhat, V.B., Bhowmik, S.K., Gupta, V., Arora, K., et al. (2016). Fatty Acid Oxidation-Driven Src Links Mitochondrial Energy Reprogramming and Oncogenic Properties in Triple-Negative Breast Cancer. Cell Rep. *14*, 2154–2165. https://doi.org/10.1016/j.celrep.2016.02.004.
7. Camarda, R., Zhou, A.Y., Kohnz, R.A., Balakrishnan, S., Mahieu, C., Anderton, B., Eyob, H., Kajimura, S., Tward, A., Krings, G., et al. (2016). Inhibition of fatty acid oxidation as a therapy for MYC-overexpressing triple-negative breast cancer. Nat. Med. *22*, 427–432. https://doi.org/10.1038/nm.4055.
8. Attri, K.S., Park, J.H., and Kaipparettu, B.A. (2022). Redox regulation of hybrid metabolic state in breast cancer metastasis. Ann. Transl. Med. *10*, 1032. https://doi.org/10.21037/atm-22-3730.
9. Ren, Z., Liang, H., Galbo, P.M., Jr., Dharmaratne, M., Kulkarni, A.S., Fard, A.T., Aoun, M.L., Martinez-Lopez, N., Suyama, K., Benard, O., et al. (2022). Redox signaling by glutathione peroxidase 2 links vascular modulation to metabolic plasticity of breast cancer. Proc. Natl. Acad. Sci. USA *119*, e2107266119. https://doi.org/10.1073/pnas.2107266119.
10. Pacella, I., Procaccini, C., Focaccetti, C., Miacci, S., Timperi, E., Faicchia, D., Severa, M., Rizzo, F., Coccia, E.M., Bonacina, F., et al. (2018). Fatty acid metabolism complements glycolysis in the selective regulatory T cell expansion during tumor growth. Proc. Natl. Acad. Sci. USA *115*, E6546–E6555. https://doi.org/10.1073/pnas.1720113115.
11. Jia, D., Lu, M., Jung, K.H., Park, J.H., Yu, L., Onuchic, J.N., Kaipparettu, B.A., and Levine, H. (2019). Elucidating cancer metabolic plasticity by coupling gene regulation with metabolic pathways. Proc. Natl. Acad. Sci. USA *116*, 3909–3918. https://doi.org/10.1073/pnas.1816391116.
12. Jia, D., Park, J.H., Kaur, H., Jung, K.H., Yang, S., Tripathi, S., Galbraith, M., Deng, Y., Jolly, M.K., Kaipparettu, B.A., et al. (2021). Towards decoding the coupled decision-making of metabolism and epithelial-to-mesenchymal transition in cancer. Br. J. Cancer *124*, 1902–1911. https://doi.org/10.1038/s41416-021-01385-y.
13. Jia, D., Park, J.H., Jung, K.H., Levine, H., and Kaipparettu, B.A. (2018). Elucidating the Metabolic Plasticity of Cancer: Mitochondrial Reprogramming and Hybrid Metabolic States. Cells *7*, 21. https://doi.org/10.3390/cells7030021.
14. Yu, L., Lu, M., Jia, D., Ma, J., Ben-Jacob, E., Levine, H., Kaipparettu, B.A., and Onuchic, J.N. (2017). Modeling the Genetic Regulation of Cancer Metabolism: Interplay between Glycolysis and Oxidative Phosphorylation. Cancer Res. *77*, 1564–1574. https://doi.org/10.1158/0008-5472.CAN-16-2074.
15. Xu, Q., Biener-Ramanujan, E., Yang, W., and Ramanujan, V.K. (2015). Targeting metabolic plasticity in breast cancer cells via mitochondrial complex I modulation. Breast Cancer Res. Treat. *150*, 43–56. https://doi.org/10.1007/s10549-015-3304-8.
16. Foretz, M., Guigas, B., and Viollet, B. (2019). Understanding the glucoregulatory mechanisms of metformin in type 2 diabetes mellitus. Nat. Rev. Endocrinol. *15*, 569–589. https://doi.org/10.1038/s41574-019-0242-2.

17. Morales, D.R., and Morris, A.D. (2015). Metformin in cancer treatment and prevention. Annu. Rev. Med. *66*, 17–29. https://doi.org/10.1146/annurev-med-062613-093128.

18. Chandel, N.S., Avizonis, D., Reczek, C.R., Weinberg, S.E., Menz, S., Neuhaus, R., Christian, S., Haegebarth, A., Algire, C., and Pollak, M. (2016). Are Metformin Doses Used in Murine Cancer Models Clinically Relevant? Cell Metab. *23*, 569–570. https://doi.org/10.1016/j.cmet.2016.03.010.

19. Hampsch, R.A., Wells, J.D., Traphagen, N.A., McCleery, C.F., Fields, J.L., Shee, K., Dillon, L.M., Pooler, D.B., Lewis, L.D., Demidenko, E., et al. (2020). AMPK Activation by Metformin Promotes Survival of Dormant ER(+) Breast Cancer Cells. Clin. Cancer Res. *26*, 3707–3719. https://doi.org/10.1158/1078-0432.CCR-20-0269.

20. Vasan, K., and Chandel, N.S. (2024). Molecular and cellular mechanisms underlying the failure of mitochondrial metabolism drugs in cancer clinical trials. J. Clin. Invest. *134*, e176736. https://doi.org/10.1172/JCI176736.

21. Dowling, R.J.O., Lam, S., Bassi, C., Mouaaz, S., Aman, A., Kiyota, T., Al-Awar, R., Goodwin, P.J., and Stambolic, V. (2016). Metformin Pharmacokinetics in Mouse Tumors: Implications for Human Therapy. Cell Metab. *23*, 567–568. https://doi.org/10.1016/j.cmet.2016.03.006.

22. Pollak, M. (2013). Potential applications for biguanides in oncology. J. Clin. Invest. *123*, 3693–3700. https://doi.org/10.1172/JCI67232.

23. Weinberg, S.E., and Chandel, N.S. (2015). Targeting mitochondria metabolism for cancer therapy. Nat. Chem. Biol. *11*, 9–15. https://doi.org/10.1038/nchembio.1712.

24. Andrzejewski, S., Siegel, P.M., and St-Pierre, J. (2018). Metabolic Profiles Associated With Metformin Efficacy in Cancer. Front. Endocrinol. *9*, 372. https://doi.org/10.3389/fendo.2018.00372.

25. Janzer, A., German, N.J., Gonzalez-Herrera, K.N., Asara, J.M., Haigis, M.C., and Struhl, K. (2014). Metformin and phenformin deplete tricarboxylic acid cycle and glycolytic intermediates during cell transformation and NTPs in cancer stem cells. Proc. Natl. Acad. Sci. USA *111*, 10574–10579. https://doi.org/10.1073/pnas.1409844111.

26. Marini, C., Bianchi, G., Buschiazzo, A., Ravera, S., Martella, R., Bottoni, G., Petretto, A., Emionite, L., Monteverde, E., Capitanio, S., et al. (2016). Divergent targets of glycolysis and oxidative phosphorylation result in additive effects of metformin and starvation in colon and breast cancer. Sci. Rep. *6*, 19569. https://doi.org/10.1038/srep19569.

27. Lord, S.R., Cheng, W.C., Liu, D., Gaude, E., Haider, S., Metcalf, T., Patel, N., Teoh, E.J., Gleeson, F., Bradley, K., et al. (2018). Integrated Pharmacodynamic Analysis Identifies Two Metabolic Adaption Pathways to Metformin in Breast Cancer. Cell Metab. *28*, 679–688.e4. https://doi.org/10.1016/j.cmet.2018.08.021.

28. Lord, S.R., Collins, J.M., Cheng, W.C., Haider, S., Wigfield, S., Gaude, E., Fielding, B.A., Pinnick, K.E., Harjes, U., Segaran, A., et al. (2020). Transcriptomic analysis of human primary breast cancer identifies fatty acid oxidation as a target for metformin. Br. J. Cancer *122*, 258–265. https://doi.org/10.1038/s41416-019-0665-5.

29. Wang, J.C., Li, G.Y., Wang, B., Han, S.X., Sun, X., Jiang, Y.N., Shen, Y.W., Zhou, C., Feng, J., Lu, S.Y., et al. (2019). Metformin inhibits metastatic breast cancer progression and improves chemosensitivity by inducing vessel normalization via PDGF-B downregulation. J. Exp. Clin. Cancer Res. *38*, 235. https://doi.org/10.1186/s13046-019-1211-2.

30. Hardie, D.G. (2013). The LKB1-AMPK pathway-friend or foe in cancer? Cancer Cell *23*, 131–132. https://doi.org/10.1016/j.ccr.2013.01.009.

31. Kim, J., Yang, G., Kim, Y., Kim, J., and Ha, J. (2016). AMPK activators: mechanisms of action and physiological activities. Exp. Mol. Med. *48*, e224. https://doi.org/10.1038/emm.2016.16.

32. Ahn, S., Park, J.H., Grimm, S.L., Piyarathna, D.W.B., Samanta, T., Putluri, V., Mezquita, D., Fuqua, S.A.W., Putluri, N., Coarfa, C., and Kaipparettu, B.A. (2024). Metabolomic Rewiring Promotes Endocrine Therapy Resistance in Breast Cancer. Cancer Res. *84*, 291–304. https://doi.org/10.1158/0008-5472.CAN-23-0184.

33. Asiedu, M.K., Barron, M., Aubry, M.C., and Wigle, D.A. (2018). Patient- and Cell Type-Specific Heterogeneity of Metformin Response. Basic Clin. Pharmacol. Toxicol. *122*, 214–222. https://doi.org/10.1111/bcpt.12898.

34. Ellis, M.J., Leddy, J., Cordingley, D., and Willer, B. (2018). A Physiological Approach to Assessment and Rehabilitation of Acute Concussion in Collegiate and Professional Athletes. Front. Neurol. *9*, 1115. https://doi.org/10.3389/fneur.2018.01115.

35. Fisman, E.Z., and Tenenbaum, A. (2021). The dual glucose-dependent insulinotropic polypeptide (GIP) and glucagon-like peptide-1 (GLP-1) receptor agonist tirzepatide: a novel cardiometabolic therapeutic prospect. Cardiovasc. Diabetol. *20*, 225. https://doi.org/10.1186/s12933-021-01412-5.

36. Erdogan, B.R., and Arioglu-Inan, E. (2024). SGLT2 inhibitors: how do they affect the cardiac cells. Mol. Cell. Biochem. *1*, 1. https://doi.org/10.1007/s11010-024-05084-z.

37. Turkoz, F.P., Solak, M., Petekkaya, I., Keskin, O., Kertmen, N., Sarici, F., Arik, Z., Babacan, T., Ozisik, Y., and Altundag, K. (2013). The prognostic impact of obesity on molecular subtypes of breast cancer in premenopausal women. J. BUON. *18*, 335–341.

38. Mustafi, D., Fernandez, S., Markiewicz, E., Fan, X., Zamora, M., Mueller, J., Brady, M.J., Conzen, S.D., and Karczmar, G.S. (2017). MRI reveals increased tumorigenesis following high fat feeding in a mouse model of triple-negative breast cancer. NMR Biomed. *30*, 1. https://doi.org/10.1002/nbm.3758.

39. Donovan, M.G., Wren, S.N., Cenker, M., Selmin, O.I., and Romagnolo, D.F. (2020). Dietary fat and obesity as modulators of breast cancer risk: Focus on DNA methylation. Br. J. Pharmacol. *177*, 1331–1350. https://doi.org/10.1111/bph.14891.

40. Tan, P.Y., and Teng, K.T. (2021). Role of dietary fat on obesity-related postmenopausal breast cancer: insights from mouse models and methodological considerations. Breast Cancer *28*, 556–571. https://doi.org/10.1007/s12282-021-01233-0.

41. Thompson, A.M. (2014). Molecular pathways: preclinical models and clinical trials with metformin in breast cancer. Clin. Cancer Res. *20*, 2508–2515. https://doi.org/10.1158/1078-0432.CCR-13-0354.

42. Chen, H., Cook, L.S., Tang, M.T.C., Hill, D.A., Wiggins, C.L., and Li, C.I. (2019). Relationship between Diabetes and Diabetes Medications and Risk of Different Molecular Subtypes of Breast Cancer. Cancer Epidemiol. Biomarkers Prev. *28*, 1802–1808. https://doi.org/10.1158/1055-9965.EPI-19-0291.

43. Liu, X., Romero, I.L., Litchfield, L.M., Lengyel, E., and Locasale, J.W. (2016). Metformin Targets Central Carbon Metabolism and Reveals Mitochondrial Requirements in Human Cancers. Cell Metab. *24*, 728–739. https://doi.org/10.1016/j.cmet.2016.09.005.

44. He, L., and Wondisford, F.E. (2015). Metformin action: concentrations matter. Cell Metab. *21*, 159–162. https://doi.org/10.1016/j.cmet.2015.01.003.

45. Wang, Y., An, H., Liu, T., Qin, C., Sesaki, H., Guo, S., Radovick, S., Hussain, M., Maheshwari, A., Wondisford, F.E., et al. (2019). Metformin Improves Mitochondrial Respiratory Activity through Activation of AMPK. Cell Rep. *29*, 1511–1523.e5. https://doi.org/10.1016/j.celrep.2019.09.070.

46. Foretz, M., Hébrard, S., Leclerc, J., Zarrinpashneh, E., Soty, M., Mithieux, G., Sakamoto, K., Andreelli, F., and Viollet, B. (2010). Metformin inhibits hepatic gluconeogenesis in mice independently of the LKB1/AMPK pathway via a decrease in hepatic energy state. J. Clin. Invest. *120*, 2355–2369. https://doi.org/10.1172/JCI40671.

47. Foretz, M., Guigas, B., Bertrand, L., Pollak, M., and Viollet, B. (2014). Metformin: from mechanisms of action to therapies. Cell Metab. *20*, 953–966. https://doi.org/10.1016/j.cmet.2014.09.018.

48. Zou, H., Luo, J., Guo, Y., Tong, T., Liu, Y., Chen, Y., Xiao, Y., Ye, L., Zhu, C., Deng, L., et al. (2023). Tyrosine kinase SRC-induced YAP1-KLF5

module regulates cancer stemness and metastasis in triple-negative breast cancer. Cell. Mol. Life Sci. *80*, 41. https://doi.org/10.1007/s00018-023-04688-w.

49. Tryfonopoulos, D., Walsh, S., Collins, D.M., Flanagan, L., Quinn, C., Corkery, B., McDermott, E.W., Evoy, D., Pierce, A., O'Donovan, N., et al. (2011). Src: a potential target for the treatment of triple-negative breast cancer. Ann. Oncol. *22*, 2234–2240. https://doi.org/10.1093/annonc/mdq757.

50. Araujo, J., and Logothetis, C. (2010). Dasatinib: a potent SRC inhibitor in clinical development for the treatment of solid tumors. Cancer Treat Rev. *36*, 492–500. https://doi.org/10.1016/j.ctrv.2010.02.015.

51. Herold, C.I., Chadaram, V., Peterson, B.L., Marcom, P.K., Hopkins, J., Kimmick, G.G., Favaro, J., Hamilton, E., Welch, R.A., Bacus, S., and Blackwell, K.L. (2011). Phase II trial of dasatinib in patients with metastatic breast cancer using real-time pharmacodynamic tissue biomarkers of Src inhibition to escalate dosing. Clin. Cancer Res. *17*, 6061–6070. https://doi.org/10.1158/1078-0432.CCR-11-1071.

52. Finn, R.S., Dering, J., Ginther, C., Wilson, C.A., Glaspy, P., Tchekmedyian, N., and Slamon, D.J. (2007). Dasatinib, an orally active small molecule inhibitor of both the src and abl kinases, selectively inhibits growth of basal-type/"triple-negative" breast cancer cell lines growing in vitro. Breast Cancer Res. Treat. *105*, 319–326. https://doi.org/10.1007/s10549-006-9463-x.

53. Gucalp, A., Sparano, J.A., Caravelli, J., Santamauro, J., Patil, S., Abbruzzi, A., Pellegrino, C., Bromberg, J., Dang, C., Theodoulou, M., et al. (2011). Phase II trial of saracatinib (AZD0530), an oral SRC-inhibitor for the treatment of patients with hormone receptor-negative metastatic breast cancer. Clin. Breast Cancer *11*, 306–311. https://doi.org/10.1016/j.clbc.2011.03.021.

54. Finn, R.S., Bengala, C., Ibrahim, N., Roché, H., Sparano, J., Strauss, L.C., Fairchild, J., Sy, O., and Goldstein, L.J. (2011). Dasatinib as a single agent in triple-negative breast cancer: results of an open-label phase 2 study. Clin. Cancer Res. *17*, 6905–6913. https://doi.org/10.1158/1078-0432.CCR-11-0288.

55. Mayer, E.L., and Krop, I.E. (2010). Advances in targeting SRC in the treatment of breast cancer and other solid malignancies. Clin. Cancer Res. *16*, 3526–3532. https://doi.org/10.1158/1078-0432.CCR-09-1834.

56. Zhang, S., and Yu, D. (2012). Targeting Src family kinases in anti-cancer therapies: turning promise into triumph. Trends Pharmacol. Sci. *33*, 122–128. https://doi.org/10.1016/j.tips.2011.11.002.

57. Viollet, B., Guigas, B., Sanz Garcia, N., Leclerc, J., Foretz, M., and Andreelli, F. (2012). Cellular and molecular mechanisms of metformin: an overview. Clin. Sci. *122*, 253–270. https://doi.org/10.1042/CS20110386.

58. Zhang, C.S., Hawley, S.A., Zong, Y., Li, M., Wang, Z., Gray, A., Ma, T., Cui, J., Feng, J.W., Zhu, M., et al. (2017). Fructose-1,6-bisphosphate and aldolase mediate glucose sensing by AMPK. Nature *548*, 112–116. https://doi.org/10.1038/nature23275.

59. Larsen, S., Rabøl, R., Hansen, C.N., Madsbad, S., Helge, J.W., and Dela, F. (2012). Metformin-treated patients with type 2 diabetes have normal mitochondrial complex I respiration. Diabetologia *55*, 443–449. https://doi.org/10.1007/s00125-011-2340-0.

60. Ma, T., Tian, X., Zhang, B., Li, M., Wang, Y., Yang, C., Wu, J., Wei, X., Qu, Q., Yu, Y., et al. (2022). Low-dose metformin targets the lysosomal AMPK pathway through PEN2. Nature *603*, 159–165. https://doi.org/10.1038/s41586-022-04431-8.

61. Nascimento Da Conceicao, V., Sun, Y., Chai, X., Ambrus, J.L., Mishra, B.B., and Singh, B.B. (2023). Metformin-induced activation of Ca(2+) signaling prevents immune infiltration/pathology in Sjogren's syndrome-prone mouse models. J. Transl. Autoimmun. *7*, 100210. https://doi.org/10.1016/j.jtauto.2023.100210.

62. Loubiere, C., Clavel, S., Gilleron, J., Harisseh, R., Fauconnier, J., Ben-Sahra, I., Kaminski, L., Laurent, K., Herkenne, S., Lacas-Gervais, S., et al. (2017). The energy disruptor metformin targets mitochondrial integrity via modification of calcium flux in cancer cells. Sci. Rep. *7*, 5040. https://doi.org/10.1038/s41598-017-05052-2.

63. Hekim, C., Ilander, M., Yan, J., Michaud, E., Smykla, R., Vähä-Koskela, M., Savola, P., Tähtinen, S., Saikko, L., Hemminki, A., et al. (2017). Dasatinib Changes Immune Cell Profiles Concomitant with Reduced Tumor Growth in Several Murine Solid Tumor Models. Cancer Immunol. Res. *5*, 157–169. https://doi.org/10.1158/2326-6066.CIR-16-0061-T.

64. Tian, J., Raffa, F.A., Dai, M., Moamer, A., Khadang, B., Hachim, I.Y., Bakdounes, K., Ali, S., Jean-Claude, B., and Lebrun, J.J. (2018). Dasatinib sensitises triple negative breast cancer cells to chemotherapy by targeting breast cancer stem cells. Br. J. Cancer *119*, 1495–1507. https://doi.org/10.1038/s41416-018-0287-3.

65. Bahman, F., Pittala, V., Haider, M., and Greish, K. (2021). Enhanced Anticancer Activity of Nanoformulation of Dasatinib against Triple-Negative Breast Cancer. J. Pers. Med, *11*, 1. https://doi.org/10.3390/jpm11060559.

66. Zong, Y., Zhang, C.S., Li, M., Wang, W., Wang, Z., Hawley, S.A., Ma, T., Feng, J.W., Tian, X., Qi, Q., et al. (2019). Hierarchical activation of compartmentalized pools of AMPK depends on severity of nutrient or energy stress. Cell Res. *29*, 460–473. https://doi.org/10.1038/s41422-019-0163-6.

67. Schneider, C.A., Rasband, W.S., and Eliceiri, K.W. (2012). NIH Image to ImageJ: 25 years of image analysis. Nat. Methods *9*, 671–675. https://doi.org/10.1038/nmeth.2089.

68. Creighton, C.J. (2008). Multiple oncogenic pathway signatures show coordinate expression patterns in human prostate tumors. PLoS One *3*, e1816. https://doi.org/10.1371/journal.pone.0001816.

69. Chen, F., Zhang, Y., Gibbons, D.L., Deneen, B., Kwiatkowski, D.J., Ittmann, M., and Creighton, C.J. (2018). Pan-Cancer Molecular Classes Transcending Tumor Lineage Across 32 Cancer Types, Multiple Data Platforms, and over 10,000 Cases. Clin. Cancer Res. *24*, 2182–2193. https://doi.org/10.1158/1078-0432.CCR-17-3378.

70. Liu, B., Ordonez-Ercan, D., Fan, Z., Edgerton, S.M., Yang, X., and Thor, A.D. (2007). Downregulation of erbB3 abrogates erbB2-mediated tamoxifen resistance in breast cancer cells. Int. J. Cancer *120*, 1874–1882. https://doi.org/10.1002/ijc.22423.

71. Liu, B., Fang, M., Schmidt, M., Lu, Y., Mendelsohn, J., and Fan, Z. (2000). Induction of apoptosis and activation of the caspase cascade by anti-EGF receptor monoclonal antibodies in DiFi human colon cancer cells do not involve the c-jun N-terminal kinase activity. Br. J. Cancer *82*, 1991–1999. https://doi.org/10.1054/bjoc.2000.1201.

72. Shan, D., Chen, L., Njardarson, J.T., Gaul, C., Ma, X., Danishefsky, S.J., and Huang, X.Y. (2005). Synthetic analogues of migrastatin that inhibit mammary tumor metastasis in mice. Proc. Natl. Acad. Sci. USA *102*, 3772–3776. https://doi.org/10.1073/pnas.0500658102.

73. Bieber, L.L., Abraham, T., and Helmrath, T. (1972). A rapid spectrophotometric assay for carnitine palmitoyltransferase. Anal. Biochem. *50*, 509–518. https://doi.org/10.1016/0003-2697(72)90061-9.

74. Ma, Y., Bai, R.K., Trieu, R., and Wong, L.J.C. (2010). Mitochondrial dysfunction in human breast cancer cells and their transmitochondrial cybrids. Biochim. Biophys. Acta *1797*, 29–37. https://doi.org/10.1016/j.bbabio.2009.07.008.

75. Frazier, A.E., and Thorburn, D.R. (2012). Biochemical analyses of the electron transport chain complexes by spectrophotometry. Methods Mol. Biol. *837*, 49–62. https://doi.org/10.1007/978-1-61779-504-6_4.

76. Bonnen, P.E., Yarham, J.W., Besse, A., Wu, P., Faqeih, E.A., Al-Asmari, A.M., Saleh, M.A.M., Eyaid, W., Hadeel, A., He, L., et al. (2013). Mutations in FBXL4 cause mitochondrial encephalopathy and a disorder of mitochondrial DNA maintenance. Am. J. Hum. Genet. *93*, 471–481. https://doi.org/10.1016/j.ajhg.2013.07.017.

77. Sachs, N., de Ligt, J., Kopper, O., Gogola, E., Bounova, G., Weeber, F., Balgobind, A.V., Wind, K., Gracanin, A., Begthel, H., et al. (2018). A Living Biobank of Breast Cancer Organoids Captures Disease

Heterogeneity. Cell *172*, 373–386.e10. https://doi.org/10.1016/j.cell.2017.11.010.

78. Mohamed, D., Elshahed, M.S., Nasr, T., Aboutaleb, N., and Zakaria, O. (2019). Novel LC-MS/MS method for analysis of metformin and canagliflozin in human plasma: application to a pharmacokinetic study. BMC Chem. *13*, 82. https://doi.org/10.1186/s13065-019-0597-4.

79. Vantaku, V., Dong, J., Ambati, C.R., Perera, D., Donepudi, S.R., Amara, C.S., Putluri, V., Ravi, S.S., Robertson, M.J., Piyarathna, D.W.B., et al. (2019). Multi-omics Integration Analysis Robustly Predicts High-Grade Patient Survival and Identifies CPT1B Effect on Fatty Acid Metabolism in Bladder Cancer. Clin. Cancer Res. *25*, 3689–3701. https://doi.org/10.1158/1078-0432.CCR-18-1515.

80. Sud, M., Fahy, E., Cotter, D., Azam, K., Vadivelu, I., Burant, C., Edison, A., Fiehn, O., Higashi, R., Nair, K.S., et al. (2016). Metabolomics Workbench: An international repository for metabolomics data and metadata, metabolite standards, protocols, tutorials and training, and analysis tools. Nucleic Acids Res. *44*, D463–D470. https://doi.org/10.1093/nar/gkv1042.

81. Mao, B., and Guo, S. (2023). Statistical Assessment of Drug Synergy from In Vivo Combination Studies Using Mouse Tumor Models. Cancer Res. Commun. *3*, 2146–2157. https://doi.org/10.1158/2767-9764.CRC-23-0243.

STAR★METHODS

KEY RESOURCES TABLE

REAGENT or RESOURCE	SOURCE	IDENTIFIER
Antibodies		
Rabbit polyclonal anti-phospho-ACC(Ser79)	Cell Signaling Technology	Cat#3661S; RRID: AB_330337
Rabbit monoclonal anti-ACC	Cell Signaling Technology	Cat#3676S; RRID: AB_2219397
Mouse monoclonal anti-β-actin	Cell Signaling Technology	Cat#3700S; RRID: AB_2242334
Rabbit monoclonal anti-phospho-AMPKα(Thr172)	Cell Signaling Technology	Cat#2535S; RRID: AB_331250
Mouse monoclonal anti-AMPKα	Cell Signaling Technology	Cat#2793S; RRID: AB_915794
Mouse monoclonal anti-CPT1A	Cell Signaling Technology	Cat#12252S; RRID: AB_2797857
Rabbit polyclonal anti-c-Myc	Cell Signaling Technology	Cat#9402S; RRID: AB_2151827
Rabbit monoclonal anti-phospho-Src(Tyr416)	Cell Signaling Technology	Cat#6943S; RRID: AB_10013641
Mouse monoclonal anti-Src	Cell Signaling Technology	Cat#2110S; RRID: AB_10691385
Rabbit polyclonal anti-phospho-CaMKK2(Ser511)	Cell Signaling Technology	Cat#12818S; RRID: AB_ 2798034
Rabbit monoclonal anti-CaMKK2	Cell Signaling Technology	Cat#16810S; RRID: AB_2798771
Rabbit monoclonal anti-PARP	Cell Signaling Technology	Cat#9532S; RRID: AB_659884
Rabbit ploYclonal anti-Vinculin	Cell Signaling Technology	Cat#4650S; RRID: AB_10559207
Rabbit monoclonal anti-CDK4	Cell Signaling Technology	Cat#12790S; RRID: AB_2631166
Rabbit monoclonal anti-phospho-beta-Catenin(Ser33/37&Thr41)	Cell Signaling Technology	Cat#9561S; RRID: AB_331729
Rabbit monoclonal anti-beta-Catenin	Cell Signaling Technology	Cat#9582S; RRID: AB_823447
Rabbit monoclonal anti-Notch2	Cell Signaling Technology	Cat#2420S; RRID: AB_2153626
Rabbit monoclonal anti-phospho-YAP1(Ser127)	Cell Signaling Technology	Cat#13008S; RRID: AB_2650553
Rabbit monoclonal anti-YAP1	ProteinTech	Cat#13584S; RRID: AB_2218915
Rabbit polyclonal-CPT2	Santa Cruz Biotechnology	Cat#sc-20671; RRID: AB_2084858
Goat anti-rabbit IgG (H + L)-HRP	Bio-Rad Laboratories	Cat#170–6515; RRID: AB_11125142
Goat anti-mouse IgG (H + L)-HRP	Bio-Rad Laboratories	Cat#170–6516; RRID: AB_11125547
Bacterial and virus strains		
Lentiviral pGIPZ-shCPT1	C-BASS	Cat#RHS4430-200245009
Lentiviral pGIPZ-shCPT1	C-BASS	Cat#RHS4430-200249720
Lentiviral pGIPZ-shCPT2	C-BASS	Cat#RHS4430-101063268
Lentiviral pGIPZ-shCPT2	C-BASS	Cat#RHS4430-200262912
Biological samples		
Patient-derived xenografts (PDX): BCM-2147, BCM-2665, BCM-3204, BCM-3561, BCM-4013, and BCM-FCP699	Patient-Derived Xenograft and Advanced *In Vivo* Models Core	https://pdxportal.research.bcm.edu/pdxportal/;jsessionid=NQ06OcQgD5SKvCUXjoqoHp33LFekMfWnwyuIbv6l.pdxportal?dswid=5325
Chemicals, peptides, and recombinant proteins		
Metformin	BioVision	Cat#1691
Phenformin	Sigma-Aldrich	Cat#P7045
Etomoxir	Sigma-Aldrich	Cat#E1905
Etomoxir	Chemgood	Cat#C1452
Ranolazine	Sigma-Aldrich	Cat#R6152
Dasatinib	Sigma-Aldrich	Cat#CDS023389
Rotenone	Sigma-Aldrich	Cat#R8875
Antimycin A	Sigma-Aldrich	Cat#A8674
3-bromopyruvate	Sigma-Aldrich	Cat#376817-M
Doxycycline	Sigma-Aldrich	Cat#D9891

(*Continued on next page*)

Continued

REAGENT or RESOURCE	SOURCE	IDENTIFIER
Crystal violet	Sigma-Aldrich	Cat#C0775
BrdU	Abcam	Cat#ab142567
5,5′-Dithiobis(2-nitrobenzoic acid) (DTNB)	Sigma-Aldrich	Cat#D8130
Palmitoyl coenzyme A lithium salt	Sigma-Aldrich	Cat#P9716
L-Carnitine hydrochloride	Sigma-Aldrich	Cat#C0283
Potassium hexacyanoferrate(III)	Sigma-Aldrich	Cat#244023
β-Nicotinamide adenine dinucleotide	Sigma-Aldrich	Cat#N7410
B-27® Supplement	Gibco	Cat#17504044
bFGF	Sigma	Cat#F0291-25UG
Heparin sodium salt	Stemcell Biotechnologies	Cat#07980
Gelatin	Sigma-Aldrich	Cat#G2500
Agarose	Denville Scientific	Cat#CA3510-6
Collagenase	Sigma-Aldrich	Cat#C9407
6-Thioguanine	Sigma-Aldrich	Cat#A4882
DMEM	GenDEPOT	Cat#CM002-050
huMEC Medium	Gibco	Cat#12753018
FBS (fetal bovine serum)	Gibco	Cat#10438026
Tet-free FBS	Takara Bio	Cat#631107
Trypsin-EDTA	GenDEPOT	Cat#CA014-010
Penicillin-Streptomycin	GenDEPOT	Cat#CA005-010
Uridine	Sigma-Aldrich	Cat#U3003
TBS Buffer (20X)	GenDEPOT	Cat#T8054-050
10X Tris-Glycine SDS buffer	GenDEPOT	Cat#T8053-050
Protease Inhibitor Cocktail	GenDEPOT	Cat#P3100-010
Phosphatase inhibitor	GenDEPOT	Cat#P3200-005
West- Q Pico Dura ECL Solution	GenDEPOT	Cat#W3653-050
Laemmli Sample Buffer(4X), Non-reducing	GenDEPOT	Cat#L1200-001
amfiSure qGreen Q-PCR Master Mix (2X), low Rox	GenDEPOT	Cat#Q5603-050
amfiRivert cDNA Synthesis Platinum Master Mix	GenDEPOT	Cat#R5600-500
Albumin	GenDEPOT	Cat#A0100-010
Skim milk	Sigma-Aldrich	Cat#1153630500
Human R-Spondin-1	Peprotech	Cat#120-38-250
Neuregulin 1 (Heregulin b-1) (human)	Peprotech	Cat#100-03
EGF	Gemini	Cat#300-110P
FGF 7 (human)	Peprotech	Cat#100-19
FGF 10 (human)	Peprotech	Cat#100-26
EGF	Peprotech	Cat#AF-100-15
Noggin (human)	Peprotech	Cat#120-10C
A83-01	Tocris	Cat#2939
Y-27632	Abmole	Cat#Y-27632
SB202190	Sigma-Aldrich	Cat#S7067
B27 supplement	Gibco	Cat#17504-44
HEPES	Invitrogen	Cat#15630-056
Primocin	Invivogen	Cat#Ant-pm-1
GlutaMax 100x	Invitrogen	Cat#35050061
Advanced DMEM/F12	Invitrogen	Cat#12634028
Matrigel phenol red free	Corning	Cat#356231
Collagenase	Sigma-Aldrich	Cat#C9407

(*Continued on next page*)

Continued

REAGENT or RESOURCE	SOURCE	IDENTIFIER
Red blood cell lysis buffer	Roche	Cat#11814389001
Corning® cell strainer	Corning	Cat#352360
Tween 20	VWR Life Science	Cat#97062-332
Nitrocellulose membrane	Bio-Rad	Cat#162-0097
High-fat diet chow	Research Diets Inc	Cat#D12492
DNase I	Sigma-Aldrich	Cat#4716728001
Liquid DAB+substrate chromogen system	Dako	Cat#K3468
Tirzepatide	Selleck Chemicals LLC	Cat#P1206
Canagliflozin	Selleck Chemicals LLC	Cat#S2760
Critical commercial assays		
Seahorse XFp cell mito stress test kit	Agilent	Cat#103010-100
Bicinchoninic Acid (BCA) protein assay Kit	GenDEPOT	Cat#P8100
QIAamp DNA Mini Kit	Qiagen	Cat#51304
RNeasy Plus Mini Kit	Qiagen	Cat#74134
Live/Dead fixable dead cell stain kit	Invitrogen	Cat# L34962
Deposited data		
RNA-Seq data for MET treatment	MDA-MB-231	GEO: GSE222767
Metabolomics data for MET treatment	SUM159	NMDR: ST003651
Experimental models: Cell lines		
Human: SUM149		N/A
Human: SUM159		N/A
Human: MDA-MB-231		N/A
Mouse: MTB-TOM		N/A
Mouse: 4T1		N/A
Human cybrid: C-A1N4		N/A
Human cybrid: C-SUM159		N/A
Human Rho0: SUM159		N/A
Experimental models: Organisms/strains		
Mouse: SCID	The Jackson Laboratory	Cat#001303
Mouse: Balb/c	The Jackson Laboratory	Cat#000651
Oligonucleotides		
Primer: Human nuclear Forward: CGACGGGAGGGTCGGGACAA, Reverse: GCCCCGCGAA AGAGCGGAAG		N/A
Primer: Human mitochondria Forward: GTCAACCTCGCTTCCCCACCCT, Reverse: TCCTGCGAATAGG CTTCCGGCT		N/A
Primer: Human CPT1A Forward: TCCAGTTGGCTTATCGTGGTG, Reverse: TCCAGAGTCCGATT GATTTTTGC		N/A
Primer: Human CPT2 Forward: CATACAAGCTACATT TCGGGACC, Reverse: AGCCCGGAGTGTCTTCAGAA		N/A
Primer: Human β-actin Forward: AGCACTGTGTTGGCCTACAG, Reverse: AGAGCTACGAGCTGCCTGAC		N/A

(*Continued on next page*)

Continued

REAGENT or RESOURCE	SOURCE	IDENTIFIER
Software and algorithms		
Prism 8	GraphPad	https://www.graphpad.com/scientific-software/prism/
Wave Desktop and Controller 2.6 Software	Agilent	https://www.agilent.com/en/product/cell-analysis/real-time-cell-metabolic-analysis/xf-software/seahorse-wave-controller-software-2-6-1-740904
ImageJ	Schneider et al.[67]	https://imagej.nih.gov/ij/
R	R Core Team	https://www.r-project.org/
Other		
PCA of Src and AMPK signature	Yu et al.[14] and Creighton et al.[68]	N/A

EXPERIMENTAL MODEL AND STUDY PARTICIPANT DETAILS

Cells

MDA-MB-231 and 4T1 cell lines were from the American Type Culture Collection (ATCC). SUM149 cell line was kindly gifted from Dr. Debeb (MD Anderson Cancer Center) and SUM159 cell line was purchased from BioIVT and also provided from Asterand Bioscience by Dr. Dave. c-Myc overexpressing MTB-TOM cell was provided by Dr. Goga (UCSF). Rho0 cell and TNBC cybrid cells, C-A1N4 and C-SUM159, were maintained as previously published.[6] MDA-MB-231, 4T1, SUM149, SUM159, and TNBC cybrid cells were cultured in DMEM medium containing 5% FBS and 1% penicillin-streptomycin and Rho0 cell was cultured in DMEM medium containing 5% FBS, 1% penicillin-streptomycin and 50 ng/ul uridine. MTB-TOM cell was maintained in DMEM medium containing 5% tet-free FBS and 1% penicillin-streptomycin. All cells were incubated at 37°C with 5% CO_2.

PDX-derived organoid (PDXO)

PDXOs were developed from the xenografts of already established TNBC PDX models obtained from the PDX core facility at Baylor College of Medicine. The PDXOs were maintained in BC organoid medium (Advanced DMEM/F12 with 250 ng/mL R-spondin-1, 5 nM neuregulin-1, 5 ng/ml FGF-7, 20 ng/ml FGF-10, 5 ng/mL EGF, 100 ng/mL noggin, 500 nM A83-10, 5 μM Y27632, 500 nM SB202190, 1X B27 supplement, 1.25 mM N-acetylcysteine, 5 mM nicotinamide, 1X Glutamax, 10 mM HEPES, 50 μg/ml primocin, and 1% Penicillin/Streptomycin). After drug treatment, the organoid growths were monitored under a microscope. All PDXOs were incubated at 37°C with 5% CO_2.

Animal experiments

All animal studies were conducted in accordance with the standard protocol (AN-6102) approved by the Institutional Animal Care and Use Committee of Baylor College of Medicine and conformed to relevant standards as described in Use of Laboratory Animals, the Guide for the Care and Use of Laboratory Animals. Animals were housed in specific pathogen-free conditions under standard laboratory conditions (20°C–22°C with defined light/dark cycle). For mammary transplantation assay, 2 x 10^5 SUM159 cells were transplanted into the fourth mammary fat pads of 4–5 weeks old SCID/Beige female mice. For the treatment study, the mice were treated with vehicle or phenformin (20 mg/kg) through IP on every alternative day. For the PDX models, small tumor pieces from PDX (BCM-2147, 2665, 3204, 3561, and 4013) were transplanted into the fourth mammary fat pads of 4–6 weeks old SCID/Beige female mice and the mice were treated with vehicle, metformin (100 or 200 mg/kg), phenformin (20 mg/kg), and ETX (50 mg/kg) through IP, and dasatinib (10 or 20 mg/kg) through oral gavage every two days. Tumors were monitored and measured manually by caliper. For spontaneous metastasis assay, 10^4 4T1 cells were transplanted into the fourth mammary fat pads of 4–5 weeks old Balb/C female mice. After tumors start to form, once the tumor size reaches approximate 500 mm^2, primary tumors were surgically removed. The mice were treated with vehicle, metformin (200 mg/kg), dasatinib (20 mg/kg) or its combination. The metastasis was monitored by animal observation and luciferase bioluminescence imaging (IVIS Lumina XR).

METHOD DETAILS

Mathematical modeling

The mathematical model was executed as described previously.[11] During the calculation of the average level of regulatory proteins (e.g., pAMPK) and metabolic pathway rates (e.g., FAO), as one set of parameters can enable n (i.e., multiple) stable states and a weight factor 1/n was added to each of the n solutions.

The correlation of Src and AMPK signature

We have previously published the gene lists of Src signature[68] and the AMPK signature.[14] From the TCGA RNA-seq data of the basal subgroup of breast cancer patients, the AMPK signature and Src-upregulated gene expressions were obtained. The RSEM expression level of each gene first underwent log2 transformation, followed by *Z* score normalization across the patients. The correlation between AMPK signature and Src up-regulated signatures was quantified using the average normalized expression of all genes in the corresponding signature.

Protein isolation and western blot analysis

Cells or tumor tissues were lysed or homogenized in ice-cold RIPA buffer with a protease inhibitor cocktail (GenDEPOT) followed by centrifugation for 10 min at 14000 rpm at 4°C. The supernatant was collected and quantified using a BCA assay kit (GenDEPOT). The samples were prepared in 1X Laemmli buffer (GenDEPOT) containing β-mercaptoethanol, and 30 μg cell lysates were loaded onto the SDS-PAGE. The electrophoresis and Western Blots were performed, followed by blocking in either 5% skimmed milk (Sigma) or 3% BSA (GenDEPOT) for 60 min. The nitrocellulose membranes were incubated with the primary antibodies (for pSrc(Y419), Src, pACC(S79), ACC, pAMPKα(T172), AMPKα, CPT-1, c-Myc, pCaMMK2(S511), CaMMK2, Non-phospho (Active) β-catenin(S33/37,T41), β-catenin, Notch2, pYAP1(S127), YAP1, CDK4, Vinculin, and β-actin) in 1:2,000 dilutions and further with secondary antibody conjugated HRP in 1:10,000 dilutions. Next, the membrane was washed three times with TBS-T buffer (GenDEPOT) and developed by ECL solution (GenDEPOT) using Azure 600 (Azure Biosystems).

RNA isolation and qRT-PCR

Total RNA was extracted using the RNeasy kit (Qiagen), and complementary DNA synthesis was performed using the amfiRivert cDNA Synthesis Platinum system (GenDEPOT) according to the manufacturer's instructions. mRNA levels were measured with gene-specific primers using the Mx3000P qPCR System (Stratagene). Relative expression was normalized to β-actin or glyceraldehyde-3-phosphate dehydrogenase (GAPDH).

RNA-seq analysis

Total RNA was extracted using the RNeasy Kit (Qiagen) by the manufacturer's instructions. RNA purity and concentration were measured using Nanodrop. Preparation of RNA library and transcriptome sequencing was conducted by Novogene Corporation Inc. The datasets were processed and analyzed using Illumina NovaSeq 6000 Sequencing System. Signatures for oncopathways such as MYC, p53, Kras, Notch, Wnt, YAP1, Cell Cycle, and Src were computed as previously described.[68,69]

Seahorse analysis

Metabolic flux was measured using XFp seahorse (Seahorse Biosciences). OCR was measured as previously described[6] with minor modifications. Cell Mito Stress kit (Seahorse Biosciences) was used for the assay. Basal OCR and ATP production were calculated by Report Generator Version: 4.03 (Seahorse Biosciences).

Cell viability assay

Cell viability was monitored after different drug treatments using the sulforhodamine B (SRB)-based colorimetric assay.[6]

Wound healing assay

For the wound healing assay, we used Cytation 5 (BioTek). The experiment was conducted as previously reported with minor modifications.[6] 2 X 10^4 cells were seeded into 96-well plates and incubated for overnight. Wounds were created using the wound maker and then monitored by Cytation 5.

Proliferation assay

Using the IncuCyte ZOOM technique or Cytation 5, a real-time proliferation assay was performed. About 2,000 cells were plated into 96-well plate and monitored for 72 h. Cell confluence was analyzed using the IncuCyte ZOOM or Cytataion 5 software.

Clonogenic assay

Clonogenic assays were performed as described previously.[70,71] In a 12 or 6-well plate, 500 or 2,000 cells were seeded in triplicates. After 24 h incubation, cells were treated with drugs and further incubated for 10 days. To measure lung metastasis from primary tumor *in vivo*, a clonogenic assay using *in vivo* lung tissues was conducted in the presence of 6-thioguanine,[72] Lung samples were finely minced and digested in 2 mL of enzyme cocktail containing 1 mg/mL collagenase for 2–3 h at 4°C on rotating wheel, followed by filtering through 70-μm nylon cell strainers, then washing three times with 1X PBS. The resulting cells were resuspended and plated serially diluted on 10-cm tissue culture dishes in a medium containing 60 μM 6-thioguanine for clonogenic growth. 6-thioguanine-resistant tumor cells formed foci within 10–14 days. The clones were fixed with a solution containing 10% acetic acid and 10% methanol and then stained with 0.5% crystal violet solution for 10 min, followed by three rinses with tap water to remove excess dye. After counting the number of clones, they were dissolved in a 10% acetic acid solution to measure absorbance at 590 nm.

Soft agar colony formation assay

Soft agar colony formation assay was performed as previously published[6] with minor modifications. 10,000 cells were seeded onto top agar of six-well plates. Colonies were counted at different intervals using the GelCount colony counting system (Oxford Optronix) according to the manufacturer's instructions.

Mammosphere forming assay

To generate mammospheres, 1,000 cells were seeded and grown in serum-free mammosphere media containing EGF, bFGF, Heparin, and B27 supplement in a 24-well low attachment plates. The suspension cultures were incubated for 2–3 weeks. Mammospheres were counted with an automated gel counter (Oxford Optronix).

Migration assay

The migration assay was performed using 5 x 10^4 cells in the 24-well Transwell inserts (Corning),[6] Medium containing 10% FBS was used as the chemo-attractant in the lower chamber. Cells which have migrated through the membrane were fixed with 100% methanol, stained with 1% crystal violet, and counted.

Immunohistochemistry staining

For H&E, Ki-67, and BrdU staining, PDX tissues were fixed in 4% paraformaldehyde overnight at 4°C and switched to 70% ethanol before embedding into paraffin blocks for sectioning. H&E staining and IHC staining were performed by Breast Center Pathology Core at Baylor College of Medicine.

CPT1 activity assay

CPT1 activity was measured by spectrophotometric assay as described previously with modifications.[73] Whole-cell lysates in a lysis buffer with 20 mM Tris-HCl (pH7.5), 150 mM NaCl, 1 mM EDTA, and 0.2% Triton X-100 were prepared. Then, the protein concentration is determined by BCA assay. 100 μg lysates were mixed with a lysis buffer containing 1 mM 5,5′-dithiobis-(2-nitrobenzoic acid) (DTNB). After 30 min pre-incubation at 30°C, the reaction was initiated for the baseline. And then, with adding the substrates of 250 μM Palmitoyl-CoA and 1 mM L-carnitine, the reaction was resumed by an immediate measurement at 412 nm. The calculation of CPT1 activity was based on absorbance and normalized with protein concentrations.

Complex I activity assay

The activities of complex I (NADH:ferricyanide reductase) was measured as previously described.[74] Cells were sonicated in cell sonication solution (250 mM Sucrose, 2 mM EDTA, and 100 mM Tris-HCl(pH7.4)) and the protein quantification of lysates was performed by Bradford assay. The activity of complex I from ETC and citrate synthase (CS) from TCA cycle was measured using appropriate electron acceptors/donors according to published procedure[75] by a Tecan Infinite M200 microplate plate reader. The assay is based on the kinetics for the conversion of substrates of individual enzyme. NADH was used as a substrate for complex I. Acetyl-CoA and oxaloacetate were used as substrates for CS. The enzyme activity data were normalized to the protein concentration.

Mitochondrial (mt) DNA copy number

Total genomic DNA was extracted from cells. To quantify mtDNA copy number, qPCR by nuclear (ND1) and mitochondrial (B2M) specific primers was performed using SYBR on ~3 ng genomic DNA according to published procedures.[76] Briefly, after determining the cycle threshold (Ct) value of a mitochondrial-specific and nuclear-specific targets, we calculated mtDNA copy number/haploid genome using the relative ΔCt value.

PDXO generation

For PDXO preparation, PDX tumor chunks were incubated in AdDF+++ media (Advance DMEM/F12 with 1X Glutamax, 10 mM HEPES, and 1% Penicillin/Streptomycin) for 10 min and washed with PBS. Minced PDX tissues were digested in BC organoid medium (Advanced DMEM/F12 with 250 ng/mL R-spondin-1, 5 nM neuregulin-1, 5 ng/ml FGF-7, 20 ng/ml FGF-10, 5 ng/mL EGF, 100 ng/mL noggin, 500 nM A83-10, 5 μM Y27632, 500 nM SB202190, 1X B27 supplement, 1.25 mM N-acetylcysteine, 5 mM nicotinamide, 1X Glutamax, 10 mM HEPES, 50 μg/ml primocin, and 1% Penicillin/Streptomycin) with collagenase. After digestion, organoids were collected through 100 μm cell strainer and cultured using Matrigel domes in 48 well plate as previously published.[77] Medium was exchanged every 3 to 4 days, and, once mature, cultures were passaged by incubating in dispase solution (20% FBS in dispase with Y-27632), followed by a wash step with base medium and a dissociation step in TrypLE Express. Single cells were seeded at 200,000–400,000 cells per dome.

Quantification of metformin

For quantification of metformin levels in tumors, tumor tissues (40 mg) were transferred to vials containing 600 μL of water. Samples were homogenized using homogenizer and centrifuged at 5,000 rpm for 10 min. Each sample was mixed with 1.2 mL of acetonitrile, and vortex for 5 min[21] After centrifugation, the sample was transferred to mass spectrometry vials. Metformin calibration standard (0.003–100 ng/mL) was used for generating the standard curve and determine the concentration of metformin. Metformin separation

was achieved on XDB-C18 (50 mm × 4.6 mm, 1.8 μm) analytical column (Agilent Technologies, Santa Clara, CA) maintained at ambient temperature. The mobile phase used was acetonitrile: 0.1% formic acid (40:60, v/v) delivered at a flow rate of 0.5 mL/min with an injection volume of 10 μL. The total LC run time was 5 min[78] The mass spectrometer was operated positive ESI mode. Quantification was accomplished through using multiple reaction monitoring (MRM) of the transitions of mass-to-charge ratio m/z 130.11 → 71.2, and m/z 130.11 → 43.2 for metformin using Agilent 6495B Triple Quadruple (Agilent, USA). The following mass spectrometry parameters were set: gas temperature = 250°C, gas flow = 14 min/L, nebulizer gas = 20 psi, sheath gas temperature = 350°C, sheath gas flow = 12 min/L. The integration of the peak and data were analyzed using Agilent Mass Hunter Quantitative Analysis software (Agilent Technologies, Santa Clara, CA).

Metabolomics

Metabolomics for carnitines from SUM159 cells treated with metformin was performed as previously described.[79] This study is available at the NIH Common Fund's National Metabolomics Data Repository (NMDR) Website, the Metabolomics Workbench,[80] https://www.metabolomicsworkbench.org where it has been assigned Study ID ST003651. The data can be accessed directly via its Project DOI: https://doi.org/10.21228/M8CC1G.

QUANTIFICATION AND STATISTICAL ANALYSIS

Unless stated otherwise, data are mean ± SEM, and the two-tailed unpaired Student's t test, one-way ANOVA, two-way ANOVA, or Mantel-Cox test was used to assess statistical significance using the GraphPad PRISM 8 software with $p < 0.05$ being regarded as significant. Statistical details of experiments were described in the figure legends. The synergism analysis of PDX tumor growth (last date) by drug combination was calculated using 'invivoSyn' package in R considering the bliss method as described in a previous publication by Mao B et al.[81]